Impaired Autonomic Regulation of Resistance Arteries in Mice With Low Vascular Endothelial Growth Factor or Upon Vascular Endothelial Growth Factor Trap Delivery

Erik Storkebaum, Carmen Ruiz de Almodovar, Merlijn Meens, Serena Zacchigna, Massimiliano Mazzone, Greet Vanhoutte, Stefan Vinckier, Katarzyna Miskiewicz, Koen Poesen, Diether Lambrechts, Ger M.J. Janssen, Gregorio E. Fazzi, Patrik Verstreken, Jody Haigh, Paul M. Schiffers, Hermann Rohrer, Annemie Van der Linden, Jo G.R. De Mey and Peter Carmeliet

The online version of this article, along with updated information and services, is located on the World Wide Web at:

http://circ.ahajournals.org/cgi/content/full/122/3/273

Data Supplement (unedited) at:

http://circ.ahajournals.org/cgi/content/full/CIRCULATIONAHA.109.929364/DC1

Molecular Cardiology

Impaired Autonomic Regulation of Resistance Arteries in Mice With Low Vascular Endothelial Growth Factor or Upon Vascular Endothelial Growth Factor Trap Delivery

Erik Storkebaum, PhD*; Carmen Ruiz de Almodovar, PhD*; Merlijn Meens, MS;
Serena Zacchigna, PhD; Massimiliano Mazzone, PhD; Greet Vanhoutte, PhD;
Stefan Vinckier, PhD; Katarzyna Miskiewicz, PhD; Koen Poesen, PhD; Diether Lambrechts, PhD;
Ger M.J. Janssen, BSc; Gregorio E. Fazzi, BSc; Patrik Verstreken, PhD; Jody Haigh, PhD;
Paul M. Schiffers, PhD; Hermann Rohrer, PhD; Annemie Van der Linden, PhD;
Jo G.R. De Mey, PhD; Peter Carmeliet, MD, PhD

Background—Control of peripheral resistance arteries by autonomic nerves is essential for the regulation of blood flow. The signals responsible for the maintenance of vascular neuroeffector mechanisms in the adult, however, remain largely unknown.

Methods and Results—Here, we report that VEGF$^{\partial/\partial}$ mice with low vascular endothelial growth factor (VEGF) levels suffer defects in the regulation of resistance arteries. These defects are due to dysfunction and structural remodeling of the neuroeffector junction, the equivalent of a synapse between autonomic nerve endings and vascular smooth muscle cells, and to an impaired contractile smooth muscle cell phenotype. Notably, short-term delivery of a VEGF inhibitor to healthy mice also resulted in functional and structural defects of neuroeffector junctions.

Conclusions—These findings uncover a novel role for VEGF in the maintenance of arterial neuroeffector function and may help us better understand how VEGF inhibitors cause vascular regulation defects in cancer patients. (***Circulation.*** 2010;122:273-281.)

Key Words: arteries ■ muscle, smooth ■ nervous system ■ vascular endothelial growth factor ■ vasoconstriction

Several cues have been identified that control the development of the sympathetic nervous system,[1] but the molecular mechanisms underlying the maintenance of autonomic innervation of peripheral resistance arteries in adulthood remain largely unknown. Periarterial nerves do not penetrate the medial vascular smooth muscle cell (SMC) layer but are confined to the media adventitia border. The varicose terminal portions of these nerve fibers release transmitter en passage,[2] and autonomic neuroeffector junctions (NEJs) in resistance arteries are "atypical" in that they contain prejunctional membrane thickenings with synaptic vesicles but lack specialized postjunctional structures.[2]

Clinical Perspective on p 281

By releasing neurotransmitters, autonomic nerves control the blood supply to organs. For instance, autonomic control of resistance arteries mediates thermoregulation in the skin and redistribution of flow from internal organs to the brain in stress conditions.[3,4] Dysfunction of the periarterial autonomic nervous control can lead to hypertension, Raynaud phenomenon, and orthostatic hypotension.[5] Impaired vascular regulation has also been implicated in the hand-foot syndrome in cancer patients receiving vascular endothelial growth factor (VEGF) inhibitors.[6] This syndrome is characterized by dysesthesia, erythema, and tingling of extremities, which may progress to burning pain with dryness, cracking, and ulceration of the skin.[7,8] The molecular basis of this syndrome remains largely enigmatic.

VEGF, a key regulator of angiogenesis in health and disease,[9] also has neurotrophic effects. VEGF stimulates axon outgrowth and survival of neurons in vitro,[10] and low VEGF levels in VEGF$^{\partial/\partial}$ mice, engineered to lack the hypoxia-response element in the VEGF promoter, cause adult-onset motoneuron degeneration, reminiscent of the human motoneuron degenerative disorder amyotrophic lateral sclerosis.[11] However, surprisingly little is known about the effects of VEGF on peripheral autonomic nerves and, in particular, about its possible role in the

autonomic innervation of resistance arteries in vivo. In vitro studies show that VEGF stimulates axon outgrowth and survival of superior cervical ganglia[12,13] and induces growth cone spreading of cultured postganglionic neurons.[14] Furthermore, VEGF promotes the reinnervation of denervated femoral arteries in vivo.[14] However, a role for VEGF in the maintenance of the perivascular autonomic nerve plexus in vivo has not been addressed. Here, we assessed whether VEGF might modulate the autonomic nervous control of resistance arteries.

Methods

Transgenic Mice and Soluble Flk1 Gene Transfer

VEGF$^{\partial/\partial}$, VEGF-LacZ, and Flt1-LacZ mice were described previously.[11,15,16] Expression of the soluble extracellular domain of Flk1 (sFlk1) in the circulation was obtained by hydroporating mice with 2.5 mL Ringer solution (150 mmol/L NaCl, 4 mmol/L KCl, 1 mmol/L CaCl$_2$) containing 50 μg per mouse of a vector encoding sFlk1 or an empty vector as control.[17] After 5 days, plasma protein levels of sFlk1 were determined with a soluble VEGF receptor-2 (VEGFR-2)–specific immunoassay (R&D Systems, Minneapolis, Minn).

Histology and Immunohistochemistry

Perfusion-fixed arteries were embedded in paraffin, and sections were stained with the following antibodies: polyclonal rabbit anti-smoothelin antibody (1:100; a gift from G. van Eys, Maastricht University), anti-desmin antibody (1:50; Cappel, Durham, NC), and anti–SM myosin heavy chain (MHC) antibody (1:400; ab683, Abcam, Cambridge, UK). Procedures used for whole-mount staining of arteries, analysis of skin vascular density, LacZ enzymatic staining, alkaline phosphatase staining, glyoxylic acid staining, and noradrenaline content determination are described in the Methods section of the online-only Data Supplement.

Isometric Wire Myography

Isometric wire myography was performed as described previously.[18] Detailed procedures can be found in the Methods section of the online-only Data Supplement.

Quantitative Real-Time Polymerase Chain Reaction Experiments

Messenger RNA transcript levels were quantified and normalized relative to the expression level of β-actin or GAPDH with the use of premade primers and probes (TaqMan Gene Expression Assays, Applied Biosystems, Foster City, Calif). Relative gene expression in VEGF$^{\partial/\partial}$ versus control arteries was calculated with the $2^{-\Delta\Delta CT}$ method.

Transmission Electron Microscopy

Standard procedures were used for transmission electron microscopy. Detailed procedures can be found in the Methods section of the online-only Data Supplement.

Thermoregulation Experiments

A rectal probe connected with a digital thermometer (Physitemp Instruments) was used to measure body temperature in an ambient temperature of 21°C on 3 consecutive days with 3 measurements per day; the average temperature was recorded as baseline. During exposure to cold stress (8°C for VEGF$^{\partial/\partial}$ mice, 4°C for sFlk1 mice), rectal temperature was measured at half-hour intervals for 4.5 hours.

Blood Flow Measurements

Details on these and other methods used in this study can be found in Methods section of the online-only Data Supplement.

Statistics

For comparison of 2 genotypes or treatment groups, the unpaired Student t test was used. When data were not normally distributed, the Mann–Whitney test was used; medians and interquartile ranges are reported. For the evaluation of body temperature evolution during cold stress experiments, repeated-measures ANOVA was used. For statistical analysis of concentration-response curves, ANOVA was used with Bonferroni correction for multiple testing. A limitation of our study is that, because of the limited availability of transgenic mice, sample size in our experiments is often small, increasing the risk for a type I error.

## Results

Expression of VEGF and VEGFRs

For VEGF to regulate the function of resistance arteries, VEGF and VEGFRs should be expressed in these arteries. We therefore determined the spatial expression pattern of VEGF and VEGFRs (VEGFR-1/Flt1 and VEGFR-2/Flk1) in mesenteric and saphenous arteries. In VEGF-LacZ mice, which express nuclear LacZ under the control of the endogenous VEGF promotor,[15] X-gal staining revealed VEGF expression by medial SMCs (Figure 1A) and by neurons in celiac and superior cervical ganglia (Figure 1B and not shown), implying that VEGF may also be released from nerve terminals. X-gal staining of arterial cross sections of Flt1-LacZ mice, which express cytosolic LacZ under the control of the endogenous Flt1 promotor,[16] revealed Flt1 expression in medial SMCs (Figure 1C). This expression pattern of Flt1 was confirmed by a VEGF-B$_{186}$-alkaline phosphatase (AP) fusion protein, which selectively binds to Flt1 (Figure 1D). Staining of whole-mount arteries with a VEGF-AP fusion protein, which binds to Flk1, Flt1, and neuropilin, revealed expression of VEGFRs also on periarterial nerves (Figure 1E), and immunostaining for Flt1 or Flk1 labeled perivascular nerve fibers and endings (Figure 1F and 1G). Thus, VEGF and VEGFRs are expressed in resistance arteries and periarterial nerves. We therefore tested whether VEGF might play a role in vascular regulation of peripheral resistance arteries.

To explore whether VEGF affected vascular regulation, we used VEGF$^{\partial/\partial}$ mice, which express reduced VEGF levels.[11] ELISA confirmed that VEGF protein levels were reduced in VEGF$^{\partial/\partial}$ arteries and ganglia (note I in the online-only Data Supplement), and immunostaining and quantitative polymerase chain reaction revealed that VEGF expression was reduced in arterial SM and postganglionic neurons (Figure I and note I of the online-only Data Supplement). Because VEGF$^{\partial/\partial}$ mice develop motoneuron degeneration beyond 5 to 7 months of age,[11] we used only presymptomatic VEGF$^{\partial/\partial}$ mice (≤3 months of age) for all experiments.

Impaired Vasoconstrictor Responses of VEGF$^{\partial/\partial}$ Resistance Arteries Ex Vivo

We then explored by isometric wire myography ex vivo whether the reduced VEGF levels in VEGF$^{\partial/\partial}$ mice impaired vascular regulation of isolated small muscular arteries (mesenteric and saphenous arteries) and large elastic arteries (common carotid artery).[18] To study whether VEGF modulates vasoregulatory responses of SMCs, we induced vasoconstriction by exposing arteries to stimuli that have direct effects on SMCs through distinct signal transduction pathways, ie, high potassium (K$^+$), angiotensin II, noradrenaline, or the thromboxane A$_2$ analog U46619. Because the contractile response of an artery depends on the intrinsic SMC properties but also on the thickness of the SMC layer (and because VEGF$^{\partial/\partial}$ arteries were generally
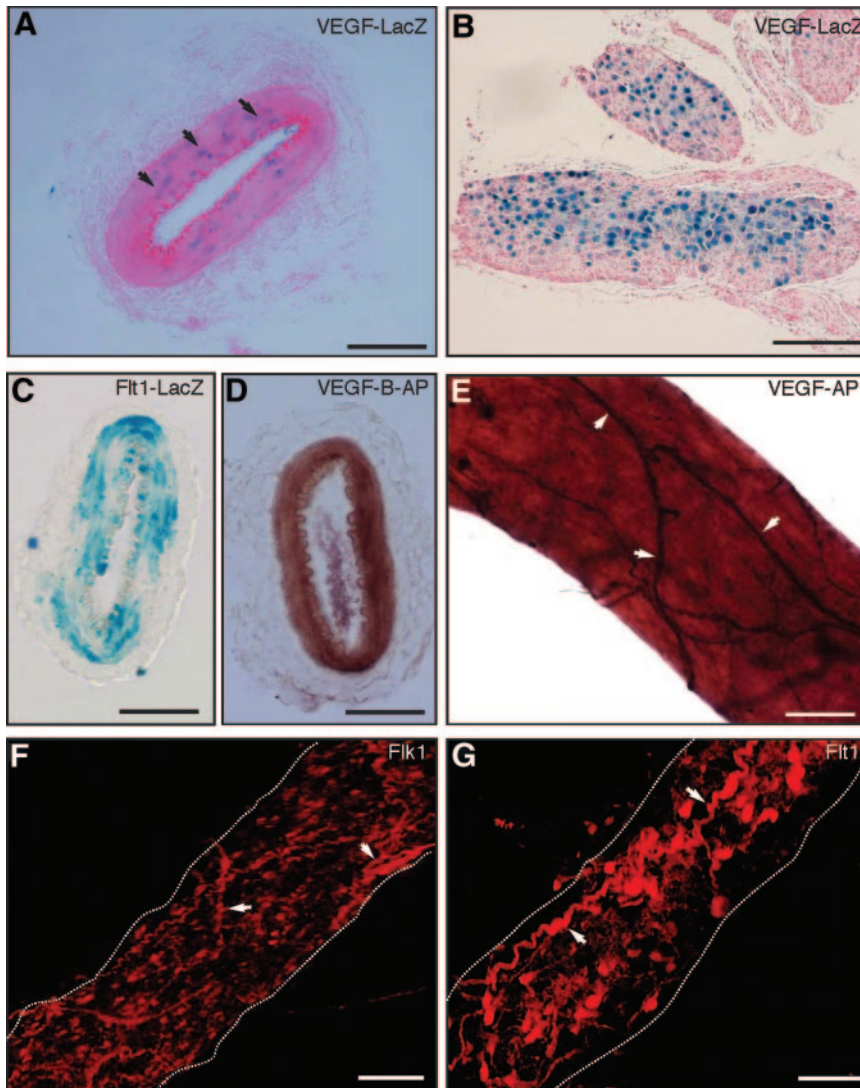
Figure 1. Expression pattern of VEGF and VEGFRs in peripheral resistance arteries. A and B, X-gal staining on saphenous arteries (A) and celiac ganglia (B) of VEGF-LacZ mice revealed VEGF expression in medial SMCs (A) (arrows, nuclear LacZ staining) and postganglionic neurons (B). C, X-gal staining on saphenous arteries of Flt1-LacZ mice revealed Flt1 expression in medial SMCs. D, Expression of Flt1 in medial SMCs was also confirmed with VEGF-B_{186}-AP fusion protein. E, Staining of whole-mount arteries with VEGF$_{164}$-AP fusion protein revealed expression of VEGFRs on periarterial nerves (arrows). F and G, Immunostaining for Flk1 (F) and Flt1 (G) on whole-mount arteries revealed expression of Flk1 and Flt1 in periarterial nerves (arrows). Scale bar=50 μm.

smaller; Table I of the online-only Data Supplement), we not only measured active wall tension (N/m), defined as the force generated by the artery divided by the arterial segment length, but also calculated active wall stress (N/m^2), a parameter of intrinsic SMC function, by correcting active wall tension for media thickness.

Compared with wild-type (WT) mice, contractile responses of resistance arteries to high K$^+$, angiotensin II, noradrenaline, or U46619 were reduced in VEGF$^{\partial/\partial}$ mice, whereas the sensitivity to these stimuli was not modified (Figure 2A, 2C, and 2D, plus Table II and Figure I of the online-only Data Supplement). Both wall tension and wall stress were reduced by >50% in VEGF$^{\partial/\partial}$ mice (Table II of the online-only Data Supplement). The fact that arterial contractility was impaired regardless of the type of vasoconstrictor stimulus indicates that SMCs were generally dysfunctional rather than having a selective defect in a particular signaling pathway. In addition, because the contractile responses were also impaired in the presence of the nitric oxide synthase inhibitor nitro-L-arginine, the defect was not attributable to abnormal production of nitric oxide (not shown). Notably, the contractile response of the elastic carotid arteries was normal (Table II and Figure IA and

ID of the online-only Data Supplement and Figure 2B), indicating that vascular regulation by densely innervated muscular arteries, but not by sparsely innervated elastic arteries, is impaired in VEGF$^{\partial/\partial}$ mice. Vascular SMC dysfunction was not accompanied by endothelial cell dysfunction because endothelium-dependent relaxation induced by acetylcholine was normal in resistance arteries of VEGF$^{\partial/\partial}$ mice (Figure II of the online-only Data Supplement).

Dedifferentiation of Vascular SMCs in VEGF$^{\partial/\partial}$ Resistance Arteries

To characterize SMC dysfunction in VEGF$^{\partial/\partial}$ arteries in more detail, we measured by quantitative polymerase chain reaction the expression of "early" and "late" SMC differentiation markers, which are important for establishing SMC contractile properties in a developmentally sequential order.[19] At 3 weeks of age, ie, when the autonomic innervation of resistance arteries was just established,[20] expression of early (nonmuscle MHC, desmin, and calponin) and late (SM MHC and smoothelin-B) SMC differentiation markers was comparable in WT and VEGF$^{\partial/\partial}$ saphenous arteries (Table 1). In contrast, by 3 months of age, expression of early SMC
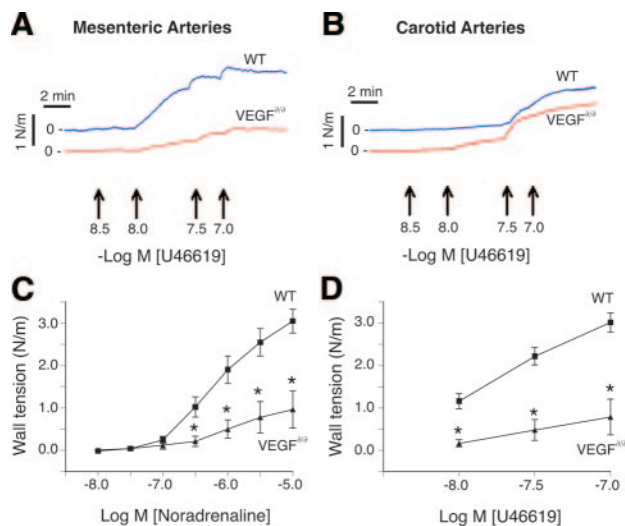
Figure 2. Impaired vascular regulation of peripheral resistance arteries in VEGF$^{\partial/\partial}$ mice. A and B, Typical recording of contractile responses to increasing concentrations of the vasoconstrictor U46619 in mesenteric resistance arteries (A) and carotid arteries (B) of WT and VEGF$^{\partial/\partial}$ mice. C and D, Concentration-response curve of WT and VEGF$^{\partial/\partial}$ saphenous arteries in response to noradrenaline (C) and U46619 (D). *$P<0.05$ vs WT.

markers was normal, but expression of the late SMC markers was reduced in VEGF$^{\partial/\partial}$ saphenous arteries (Table 1).

These results were confirmed by immunostaining (Figure III of the online-only Data Supplement). No differences were found in the expression of SMC differentiation markers in common carotid arteries (Table 1). The reduced expression of

Table 1.   Relative Expression Levels of SMC Differentiation Markers

Age	Artery	Target Gene	WT	VEGF$^{\partial/\partial}$
3 wk	SA	Nonmuscle MHC	100±14.1	78.7±19.8
		Desmin	100±14.7	71.4±13.1
		Calponin	100±13.5	63.8±18.3
		SM-MHC	100±14.1	78.6±19.8
		Smoothelin	100±19.3	118.4±35.7
3 wk	cCA	Nonmuscle MHC	100±35.4	67.4±26.9
		Desmin	100±47.3	156.5±55.2
		Calponin	100±44.1	108.7±59.8
		SM-MHC	100±35.6	67.3±26.7
		Smoothelin	100±37.0	63.0±22.3
3 mo	SA	Nonmuscle MHC	100±16.3	109.1±19.7
		Desmin	100±17.9	84.6±11.7
		Calponin	100±8.8	75.8±12.4
		SM-MHC	100±18.5	51.0±9.4*
		Smoothelin	100±14.2	49.2±9.8*
3 mo	cCA	Desmin	100±8.8	143.5±26.4
		Calponin	100±10.1	86.5±23.2
		SM-MHC	100±14.6	117.6±27.2
		Smoothelin	100±45.2	96.0±29.5

SA indicates saphenous artery; cCA, common carotid artery. Relative expression levels as percentage of WT±SEM are shown.

*$P<0.05$ versus WT.

late SMC differentiation markers in VEGF$^{\partial/\partial}$ arteries can explain their generally impaired contractile properties. This defect appeared to be specific for the contractile machinery because expression of postjunctional neurotransmitter receptors (α_1-adrenoreceptors, purinergic receptor P2X$_1$, and NPY$_1$ receptor) and neurotrophic factors (nerve growth factor, artemin, and neurotrophin-3) was not significantly altered in VEGF$^{\partial/\partial}$ arteries (not shown). Thus, SMCs in innervated resistance arteries differentiate normally during postnatal development but later dedifferentiate in VEGF$^{\partial/\partial}$ mice.

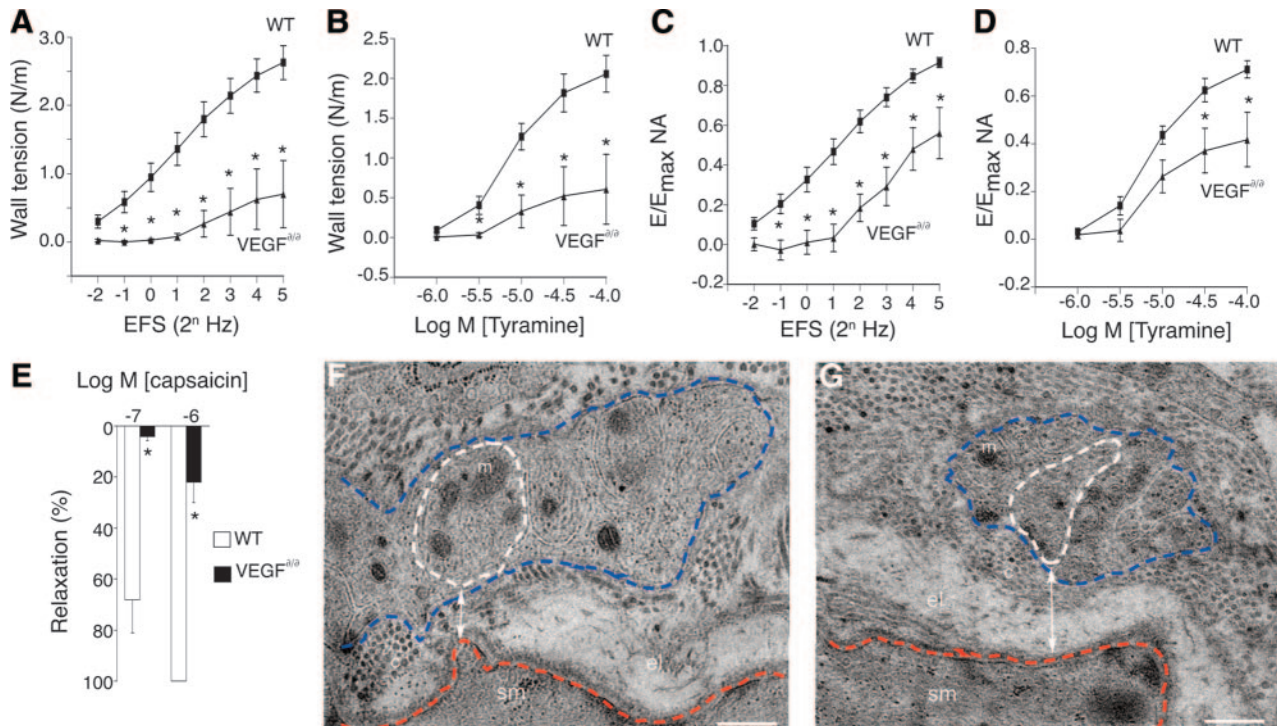**Neuroeffector Dysfunction in VEGF$^{\partial/\partial}$ Arteries**
Because vascular regulation was impaired in densely innervated, but not in sparsely innervated, arteries in VEGF$^{\partial/\partial}$ mice, suggesting a possible dysfunction of perivascular nerves, we studied neuroeffector function by ex vivo myography. In mesenteric arteries of WT mice, electric field stimulation (EFS) or administration of the indirectly acting sympathomimetic tyramine induced a strong vasoconstrictor response (Figure 3A and 3B). In contrast, the contractile response was severely impaired in VEGF$^{\partial/\partial}$ arteries (Figure 3A and 3B). To exclude that the impaired response to these neurogenic stimuli in VEGF$^{\partial/\partial}$ mice reflected only intrinsic SMC (and not neuronal) defects, we expressed the responses as a fraction of the maximal response to exogenously applied noradrenaline. Even after normalization, the contractile response remained lower in VEGF$^{\partial/\partial}$ mice (Figure 3C and 3D and Table 2), indicating that sympathetic neuroeffector regulation was dysfunctional.

Because high K$^+$ induces vasoconstriction via effects on SMCs and nerve terminals, the neuronal contribution to this response can be evaluated by measuring the relaxation induced by blocking postjunctional α-adrenoreceptors by phentolamine. The phentolamine-induced relaxation of the contractile response to K$^+$ was smaller in VEGF$^{\partial/\partial}$ arteries (Table 2), suggesting that less noradrenaline reached and activated postjunctional α-adrenoreceptors. Overall, besides general SMC hyporesponsiveness, control of vasomotor tone by sympathetic nerves was defective in VEGF$^{\partial/\partial}$ arteries. Vasorelaxation by afferent sensory-motor nerves[18] was also impaired in VEGF$^{\partial/\partial}$ arteries (Figure 3E), indicating that dysfunction of neuroeffector mechanisms involves both sympathetic and sensory-motor nerves.

Cellular Mechanisms of Neuroeffector Dysfunction in VEGF$^{\partial/\partial}$ Mice
We then sought to explore the underlying mechanisms of the perivascular nerve dysfunction. Whole-mount staining for tyrosine hydroxylase, noradrenaline, or calcitonin-gene related peptide revealed that the neuroeffector dysfunction was not attributable to a reduced density of the periarterial nervous plexus (Figure IV of the online-only Data Supplement). Additionally, the noradrenaline content of VEGF$^{\partial/\partial}$ resistance arteries was not different from that of controls (Table III of the online-only Data Supplement). We further analyzed by myography the effect of cocaine on the arterial response to exogenous noradrenaline to assess how efficiently noradrenaline reuptake by nerve terminals in situ occurred. Indeed, if noradrenaline uptake is important, blockade of this process by cocaine should leave more neurotransmitter available to activate postjunctional

Figure 3. Neuroeffector dysfunction in VEGF$^{a/a}$ arteries. A and B, Active wall tension in response to EFS (A) and tyramine (B) of WT and VEGF$^{a/a}$ arteries. C and D, Even when normalized to the maximal response to noradrenaline (NA), contractile responses to EFS (C) and tyramine (D) were reduced in VEGF$^{a/a}$ arteries. E, To monitor sensory motor nerve function, we recorded the relaxing responses to capsaicin (0.1 and 1.0 μmol/L), which selectively stimulates neurotransmitter release from sensory-motor nerve endings, in mesenteric resistance arteries that were first contracted by U46619. Capsaicin caused a substantial vasorelaxation in WT arteries, but its relaxing activity was markedly impaired in VEGF$^{a/a}$ mice (E). The sensitivity of VEGF$^{a/a}$ arteries to exogenous CGRP was not reduced (not shown), indicating that the vasorelaxation defect was attributable to sensory-motor nerve dysfunction. F and G, Representative transmission electron microscopy pictures of NEJs in VEGF$^{a/a}$ (G) and control (F) arteries illustrating wider junctional clefts and fewer mitochondria per varicosity in VEGF$^{a/a}$ arteries. Dotted lines delineate axon bundles (blue), a varicosity (white), and SMCs (red). The junctional cleft width is indicated by an arrow. c Indicates collagen; el, external elastic lamina; m, mitochondria; and sm, SMC. Scale bar=0.5 μm. *$P<0.05$ vs WT.

receptors at the NEJ. Notably, cocaine enhanced the sensitivity of VEGF$^{a/a}$ arteries to noradrenaline, but much less than that of WT arteries (Table 2). Hyporesponsiveness to cocaine in this experimental condition might reflect impaired noradrenaline uptake per se but also could be due to a wider junctional cleft between nerve varicosities and SMCs because local neurotransmitter concentrations can be influenced more readily by uptake processes in narrow junctional clefts. To discriminate between these possibilities, we measured the neuronal uptake of noradrenaline directly. Notably, no differences in noradrenaline

uptake between VEGF$^{a/a}$ and WT arteries were found (note II in the online-only Data Supplement).

We therefore explored whether the junctional cleft between perivascular nerve varicosities and target vascular SMCs might be wider. To identify structural abnormalities of VEGF$^{a/a}$ NEJs, transmission electron microscopy was used (Table 3 and Figure 3F and 3G). Morphometric quantification revealed that the distance between varicosities and the nearest SMC was larger in VEGF$^{a/a}$ arteries (Table 3). Furthermore, varicosities were smaller and contained fewer mitochondria, and axon bundles contained fewer varicosities in VEGF$^{a/a}$ arteries, whereas the density of transmitter storage vesicles was not altered (Table 3). Thus, neuroeffector dysfunction in VEGF$^{a/a}$ arteries was accompanied by structural changes in NEJs in 3-month-old mice.

To assess whether these structural changes occurred during development or only after formation of the adult periarterial nervous network, we repeated the ultrastructural analysis on arteries of 3-week-old mice in which the periarterial nerve plexus had just matured.[20] Even at this stage, the average distance between nerve varicosities and SMCs was increased in VEGF$^{a/a}$ arteries, whereas the varicosity area, number of mitochondria per varicosity, and number of varicosities per nerve bundle were reduced in VEGF$^{a/a}$ arteries (Table 3). Thus, low VEGF levels in VEGF$^{a/a}$ mice perturb normal development of arterial NEJs.

Table 2.   Sympathetic Neuroeffector Function in Saphenous Arteries

Index	Unit	WT	VEGF$^{a/a}$
EFS	E_{max}/E_{max}-(NA)	0.947 ± 0.108	0.479 ± 0.129*
Tyramine	E_{max}/E_{max}-(NA)	0.712 ± 0.036	0.326 ± 0.089*
Cocaine	ΔpD_2 NA	0.490 ± 0.077	0.100 ± 0.230*
Phentolamine	% Relaxation of contractile response to 125 mmol/L K$^+$	13.8 ± 1.7	6.4 ± 6.3*

NA indicates exogenously applied NA; E_{max}, maximal response; pD_2, $-\log M$ EC_{50} (EC_{50} is concentration resulting in 50% of E_{max}); and ΔpD_2, increase in sensitivity resulting from blockade of neuronal uptake. The data represent mean$\pm$SEM of 5 measurements.

*$P<0.05$ versus WT.

Table 3. Ultrastructural Parameters of Perivascular NEJs

Age	Artery	Parameter	WT	VEGF$^{a/a}$
3 mo	Mesenteric	Junctional cleft width	1.93±0.12	3.30±0.32*
		No. of mitochondria/varicosity	2.74±0.37	1.43±0.13*
		Varicosity area	0.83±0.11	0.36±0.048*
		No. of varicosities/axon bundle	2.78±0.22	2.12±0.14*
		transmitter vesicle density	137±20	134±27
3 mo	Saphenous	Junctional cleft width	1.49±0.045	1.90±0.17*
		No. of mitochondria/varicosity	2.17±0.24	1.51±0.16*
		Varicosity area	0.55±0.083	0.26±0.024*
		No. of varicosities/axon bundle	3.15±0.19	2.36±0.14*
3 wk	Mesenteric	Junctional cleft width	0.82±0.065	1.14±0.029*
		No. of mitochondria/varicosity	3.10±0.45	1.94±0.24*
		Varicosity area	0.65±0.080	0.32±0.042*
		No. of varicosities/axon bundle	4.57±0.46	3.29±0.23*

The data represent mean±SEM of measurements of the distance between nerve varicosities and SMCs (junctional cleft width in μm), number of mitochondria per varicosity, varicosity area (μm^2), number of varicosities per axon bundle, and transmitter storage vesicle density (μm^2).

*$P<0.05$ vs WT.

Impaired Vascular Regulation of Resistance Arteries in VEGF$^{a/a}$ Mice In Vivo

To assess whether the aforementioned ex vivo changes in neuroeffector function also impaired autonomic nervous control of peripheral resistance arteries in vivo, we explored whether thermoregulation, known to rely on autonomic nervous control of resistance arteries in the skin,[3] was impaired in VEGF$^{a/a}$ mice. In baseline conditions, the core body temperature was 38.2±0.1°C in adult WT mice but only 37.2±0.2°C in VEGF$^{a/a}$ mice (n=8; $P<0.005$). When exposed to cold stress (8°C), VEGF$^{a/a}$ mice were unable to maintain their body temperature and progressively cooled down to 34.2±1.1°C after 4.5 hours (n=8; $P=0.002$; Figure 4A). This thermoregulatory defect was not attributable to genotypic differences in blood pressure or heart rate (Table IV of the online-only Data Supplement), thyroid function (note III of the online-only Data Supplement), cutaneous vascular density (percent of surface area covered by vasculature: 29.3±1.4 in WT mice versus 29.7±1.0 in VEGF$^{a/a}$ mice; n=3; $P=0.83$), skeletal muscle dysfunction, or brown fat tissue mass (not shown).

To further evaluate whether the ex vivo peripheral arterial defects were also relevant in vivo, we analyzed whether VEGF$^{a/a}$ mice were capable of increasing cerebral blood flow (CBF) in conditions of general oxygen shortage. Indeed, when oxygen delivery to the brain becomes limiting, neurogenic constriction of resistance arteries in visceral organs ensures that brain perfusion is increased at the expense of peripheral organs.[4] We therefore exposed anesthetized ventilated mice to a brief pulse of 8% oxygen (200 seconds) and measured changes in CBF using continuous arterial spin labeling. As expected, after the hypoxic challenge, CBF was increased in WT mice by 33% (Figure 4B). In contrast, the CBF in VEGF$^{a/a}$ mice was increased by only 9% (n=4; $P<0.01$; Figure 4B). Thus, the ex vivo documented defects in vascular regulation of peripheral resistance arteries have in vivo physiological consequences.
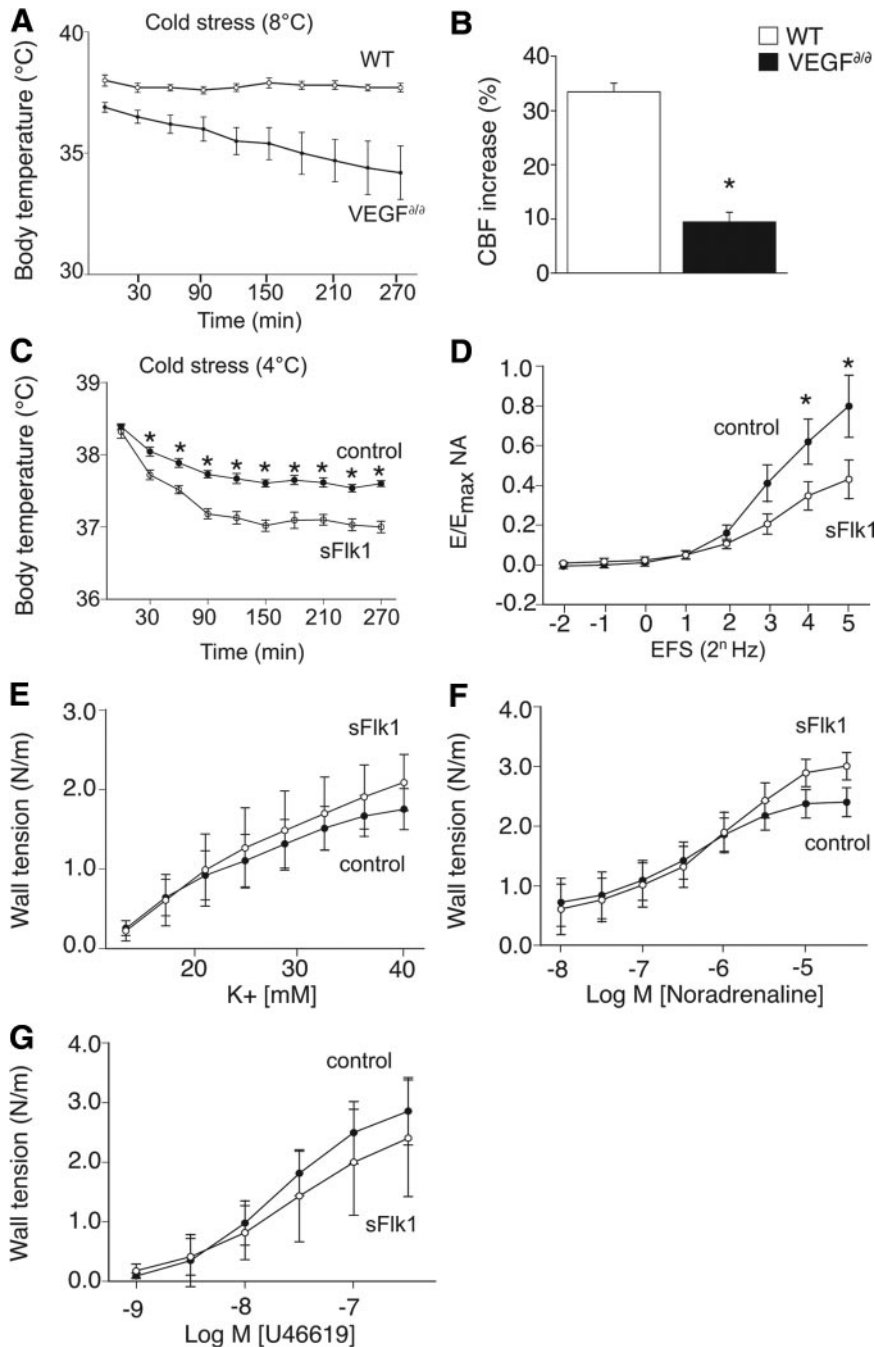
Inhibition of VEGF Impairs Vascular Regulation in WT Mice

We then assessed whether the functional and structural defects of arterial NEJs could also be induced on short-term inhibition of VEGF in adult WT mice because this would provide insight into whether VEGF might be involved in the dynamic regulation of these junctions. We therefore hydroporated WT mice with a plasmid encoding sFlk1, which traps VEGF, or an empty plasmid as control. This strategy yields high plasma levels of this VEGF inhibitor for several weeks.[17] Five days after sFlk1 gene transfer, plasma sFlk1 levels ranged from 500 to 4000 ng/mL, sufficient to inhibit VEGF-driven tumor growth.[17] Notably, ELISA measurements, using mesenteric and saphenous arteries after saline perfusion to remove intravascular sFlk1, revealed that sFlk1 diffused into the arterial wall (note IV of the online-only Data Supplement).

To evaluate the functional consequences of short-term VEGF blockade, we analyzed whether sFlk1 gene transfer in WT mice (sFlk1 mice) induced the same phenotypic defects as observed in VEGF$^{a/a}$ mice. Already 10 days after sFlk1 gene transfer, sFlk1 mice could not maintain their body temperature on exposure to cold stress (4°C during 4.5 hours; n=9 to 12; $P<0.001$; Figure 4C). In addition, the response of isolated saphenous arteries to EFS was impaired in sFlk1 mice, indicating that NEJs were dysfunctional (maximal contractile response expressed as percent of maximal response to noradrenaline: 43.0±9.8% in sFlk1 mice versus 79.8±15.6% in controls; n=7; $P=0.0008$; Figure 4D). However, different from VEGF$^{a/a}$ mice, contractile SMC responses to high potassium, noradrenaline, or U46619 (Figure 4E through 4G) and expression of SMC markers (Table V of the online-only Data Supplement) were not altered in resistance arteries of sFlk1 mice. Control of vascular regulation by endothelial cells was also normal in sFlk1 mice (Figure V of the online-only Data Supplement). Ultrastructural analysis of mesenteric resistance arteries revealed an increase in the distance between neuronal varicosities and SMCs by ≈75% in sFlk1 arteries, as well as a reduction in the number of varicosities per axon bundle by ≈30% (Table VI of the online-only Data Supplement). The area of the varicosities and the number of mitochondria per varicosity were not significantly affected by sFlk1 (Table VI of the online-only Data Supplement). Together, these results show that even short-term treatment of adult mice with a VEGF inhibitor was sufficient to induce functional and structural changes in arterial NEJs without affecting SMC function.

Discussion

The present study provides genetic evidence that subnormal VEGF levels in VEGF$^{a/a}$ mice impair vascular regulation of resistance arteries, thereby hindering thermoregulation and a compensatory increase in cerebral perfusion in response to

Figure 4. Impaired vascular regulation of resistance arteries in VEGF$^{a/a}$ or WT mice on delivery of a VEGF trap. A, Evolution of body temperature after exposure of VEGF$^{a/a}$ and WT mice to cold stress (8°C) for 4.5 hours. B, Impaired increase in CBF in VEGF$^{a/a}$ mice in response to hypoxia. C, Evolution of body temperature of mice, hydroporated with sFlk1 or empty (control) plasmid, during exposure to cold stress (4°C for 4.5 hours). D, Contraction of saphenous arteries of sFlk1 and control mice in response to EFS. E through G, Concentration-response curve of sFlk1 and control saphenous arteries in response to high potassium (E), noradrenaline (F), and U46619 (G). *$P<0.05$ vs WT.

hypoxia. Pharmacological, expression, and morphological studies further revealed that this is due to dysfunction of arterial NEJs and to dedifferentiation of contractile SMCs. Moreover, short-term inhibition of VEGF in healthy mice caused neuroeffector dysfunction without SMC defects.

Neuroeffector dysfunction was not due to overt degeneration of periarterial nerves but rather to more subtle ultrastructural defects. Indeed, the junctional cleft between nerve varicosities and target vascular SMCs was widened in VEGF$^{a/a}$ arteries, thereby lowering the fraction of released neurotransmitter, reaching and activating postjunctional receptors on target SMCs, and thus impairing neuroeffector function.[21] In addition, perivascular nerves had smaller and fewer varicosities, and these varicosities contained fewer

mitochondria. These defects may further contribute to the impaired neuroeffector function.

Vascular SMC dysfunction in VEGF$^{a/a}$ mice was associated with reduced levels of late vascular SMC differentiation markers (smoothelin-B, SM-MHC), which are typically expressed by contractile arteries.[19] So far, VEGF has been shown to stimulate SMC migration and to regulate the association of SMCs around endothelial cells[22,23] but has not been reported to regulate vascular SMC differentiation. Our findings suggest that VEGF is required to maintain SMCs in a fully differentiated contractile state. Whether this activity of VEGF relies on a direct effect on SMCs or on an indirect effect through production of "arterializing" signals from the nerve terminal remains to be determined.
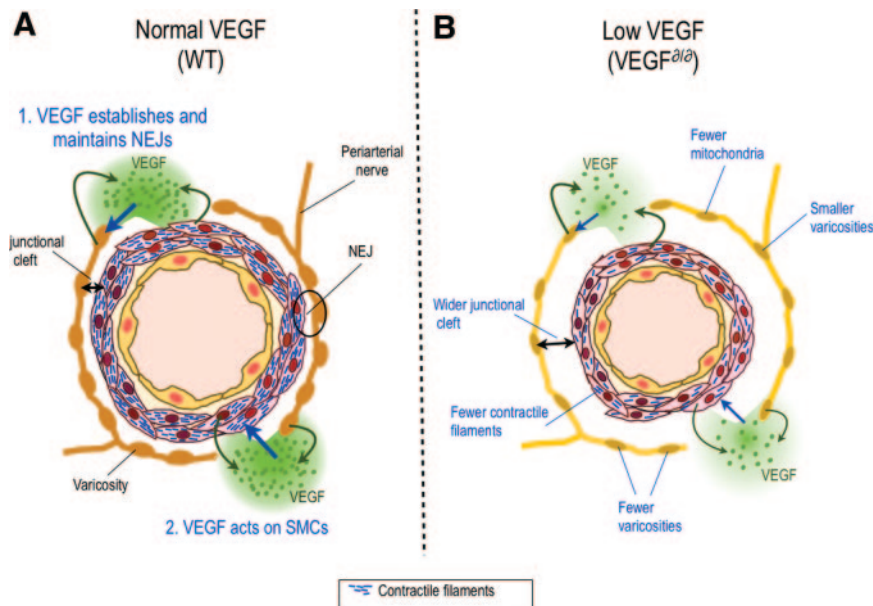
Figure 5. Role of VEGF in the maintenance of arterial neuroeffector function. A, In normal conditions, VEGF is released from SMCs and periarterial nerve endings and acts on nerve terminals to maintain NEJs (1). Another nonexclusive possibility is that VEGF primarily maintains SMCs in a differentiated state, which secondarily preserves NEJ structure and function (2). B, In VEGF$^{a/a}$ mice, low VEGF levels cause functional and structural defects of NEJs and SMC dedifferentiation.

Several mechanistic models could explain the impaired vascular regulation of VEGF$^{a/a}$ arteries (Figure 5). One model, which we favor at present, postulates that reduced release of VEGF by SMCs causes functional and structural defects of the NEJ through direct effects on the nerve terminal, which would secondarily cause SMC dedifferentiation ("prejunctional" mechanism). Arguments in favor of this model are that VEGF is expressed by vascular SMCs, that VEGF levels are reduced in VEGF$^{a/a}$ arteries, and that VEGF receptors are expressed by periarterial nerves. A primary neuronal defect is also suggested by findings that neuroeffector defects are already present by 3 weeks of age, whereas SMC differentiation is still normal. Furthermore, sFlk1 gene transfer in adult WT mice caused structural and functional neuroeffector changes without inducing SMC alterations. Previous studies documented that cultured sympathetic neurons express VEGFRs and respond to VEGF by enhanced axon outgrowth and survival,[12] but so far, VEGF has not been reported to induce structural changes in prejunctional nerve terminals. Because autonomic nerve endings are known to release SMC-trophic factors,[24] a dysfunction of these nerve terminals may secondarily lead to SMC dedifferentiation. Indeed, activation of α_1-adrenoreceptors by noradrenaline stimulates SMC proliferation,[25] and sympathetic innervation increases vascular SMC contractile protein expression,[24] whereas sympathectomy results in a switch from a contractile to synthetic SMC phenotype.[26]

An alternative nonexclusive model postulates that reduced release of VEGF from nerve endings and/or vascular SMCs could lead to SMC dedifferentiation, which would then secondarily cause defects in neuroeffector structure and function ("postjunctional" mechanism). Indeed, vascular SMCs are known to promote survival of cultured postganglionic sympathetic neurons.[27] This model seems less likely because SMC differentiation is normal in young VEGF$^{a/a}$ mice and adult sFlk1 mice in which neuroeffector defects are already present. Furthermore, quantitative polymerase chain reaction analysis revealed that the expression of nerve growth factor, artemin, and

neurotrophin-3 (known to have plasticity effects on perivascular autonomic nerves[28]) was not reduced in VEGF$^{a/a}$ arteries. Thus, we have little evidence to support a model whereby prejunctional nerve terminals, through paracrine release of VEGF, would ensure their own performance by inducing retrograde release of neurotrophic cues by target SMCs. We are therefore inclined to propose that VEGF may, at least in part, regulate the remodeling of the NEJ through direct neurotrophic effects on the prejunctional nerve terminals.

Short-term administration of the VEGF inhibitor sFlk1 to healthy adult mice was sufficient to cause vascular regulation defects and perivascular nerve dysfunction, indicating a role for VEGF in the maintenance of NEJs. An intriguing question is whether the observed functional and structural remodeling of the NEJs reflects a role for VEGF in regulating the "plasticity" of the perivascular autonomic nervous system and whether a similar role for VEGF in regulating "synaptic plasticity" exists in the central nervous system. Reports that VEGF stimulates long-term potentiation in the hippocampus would be consistent with such a model.[29] These findings also raise the intriguing but unanswered question of whether impaired vascular regulation might explain, at least in part, the hand-foot syndrome in the treatment of cancer patients with VEGF (receptor) inhibitors.[6] Indeed, impaired vascular regulation has been proposed to contribute to the hand-foot syndrome because dilated blood vessels are commonly found in affected tissues,[8] and decreasing blood flow by cooling hands and feet lowers the incidence of the hand-foot syndrome.[30] Overall, our genetic and pharmacological studies uncover a previously unrecognized role of VEGF in the proper functioning and dynamic remodeling of perivascular autonomic NEJs.

Disclosures

None.

References

1. Glebova NO, Ginty DD. Growth and survival signals controlling sympathetic nervous system development. *Annu Rev Neurosci*. 2005;28:191–222.
2. Burnstock G. Non-synaptic transmission at autonomic neuroeffector junctions. *Neurochem Int*. 2008;52:14–25.
3. Romanovsky AA. Thermoregulation: some concepts have changed: functional architecture of the thermoregulatory system. *Am J Physiol Regul Integr Comp Physiol*. 2007;292:R37–R46.
4. Kuwahira I, Gonzalez NC, Heisler N, Piiper J. Changes in regional blood flow distribution and oxygen supply during hypoxia in conscious rats. *J Appl Physiol*. 1993;74:211–214.
5. Goldstein DS, Robertson D, Esler M, Straus SE, Eisenhofer G. Dysautonomias: clinical disorders of the autonomic nervous system. *Ann Intern Med*. 2002;137:753–763.
6. Verheul HM, Pinedo HM. Possible molecular mechanisms involved in the toxicity of angiogenesis inhibition. *Nat Rev Cancer*. 2007;7:475–485.
7. Webster-Gandy JD, How C, Harrold K. Palmar-plantar erythrodysesthesia (PPE): a literature review with commentary on experience in a cancer centre. *Eur J Oncol Nurs*. 2007;11:238–246.
8. Lassere Y, Hoff P. Management of hand-foot syndrome in patients treated with capecitabine (Xeloda). *Eur J Oncol Nurs*. 2004;8(suppl 1):S31–S40.
9. Carmeliet P. Angiogenesis in life, disease and medicine. *Nature*. 2005;438:932–936.
10. Storkebaum E, Lambrechts D, Carmeliet P. VEGF: once regarded as a specific angiogenic factor, now implicated in neuroprotection. *Bioessays*. 2004;26:943–954.
11. Oosthuyse B, Moons L, Storkebaum E, Beck H, Nuyens D, Brusselmans K, Dorpe JV, Hellings P, Gorselink M, Heymans S, Theilmeier G, Dewerchin M, Laudenbach V, Vermylen P, Raat H, Acker T, Vleminckx V, Bosch LV, Cashman N, Fujisawa H, Drost MR, Sciot R, Bruyninckx F, Hicklin DJ, Ince C, Gressens P, Lupu F, Plate KH, Robberecht W, Herbert JM, Collen D, Carmeliet P. Deletion of the hypoxia-response element in the vascular endothelial growth factor promoter causes motor neuron degeneration. *Nat Genet*. 2001;28:131–138.
12. Sondell M, Lundborg G, Kanje M. Vascular endothelial growth factor has neurotrophic activity and stimulates axonal outgrowth, enhancing cell survival and Schwann cell proliferation in the peripheral nervous system. *J Neurosci*. 1999;19:5731–5740.
13. Long JB, Jay SM, Segal SS, Madri JA. VEGF-A and Semaphorin3A: modulators of vascular sympathetic innervation. *Dev Biol*. 2009;334:119–132.
14. Marko SB, Damon DH. VEGF promotes vascular sympathetic innervation. *Am J Physiol Heart Circ Physiol*. 2008;294:H2646–H2652.
15. Miquerol L, Gertsenstein M, Harpal K, Rossant J, Nagy A. Multiple developmental roles of VEGF suggested by a LacZ-tagged allele. *Dev Biol*. 1999;212:307–322.
16. Fong GH, Klingensmith J, Wood CR, Rossant J, Breitman ML. Regulation of flt-1 expression during mouse embryogenesis suggests a role in the establishment of vascular endothelium. *Dev Dyn*. 1996;207:1–10.
17. Fischer C, Jonckx B, Mazzone M, Zacchigna S, Loges S, Pattarini L, Chorianopoulos E, Liesenborghs L, Koch M, De Mol M, Autiero M, Wyns S, Plaisance S, Moons L, van Rooijen N, Giacca M, Stassen JM, Dewerchin M, Collen D, Carmeliet P. Anti-PlGF inhibits growth of VEGF(R)-inhibitor-resistant tumors without affecting healthy vessels. *Cell*. 2007;131:463–475.
18. De Mey JG, Megens R, Fazzi GE. Functional antagonism between endogenous neuropeptide Y and calcitonin gene-related peptide in mesenteric resistance arteries. *J Pharmacol Exp Ther*. 2008;324:930–937.
19. Owens GK. Regulation of differentiation of vascular smooth muscle cells. *Physiol Rev*. 1995;75:487–517.
20. Luff SE. Development of neuromuscular junctions on small mesenteric arteries of the rat. *J Neurocytol*. 1999;28:47–62.
21. Bennett MR. Autonomic neuromuscular transmission at a varicosity. *Prog Neurobiol*. 1996;50:505–532.
22. Wang H, Keiser JA. Vascular endothelial growth factor upregulates the expression of matrix metalloproteinases in vascular smooth muscle cells: role of flt-1. *Circ Res*. 1998;83:832–840.
23. Greenberg JI, Shields DJ, Barillas SG, Acevedo LM, Murphy E, Huang J, Scheppke L, Stockmann C, Johnson RS, Angle N, Cheresh DA. A role for VEGF as a negative regulator of pericyte function and vessel maturation. *Nature*. 2008;456:809–813.
24. Damon DH. Sympathetic innervation promotes vascular smooth muscle differentiation. *Am J Physiol Heart Circ Physiol*. 2005;288:H2785–H2791.
25. van Kleef EM, Smits JF, De Mey JG, Cleutjens JP, Lombardi DM, Schwartz SM, Daemen MJ. Alpha 1-adrenoreceptor blockade reduces the angiotensin II-induced vascular smooth muscle cell DNA synthesis in the rat thoracic aorta and carotid artery. *Circ Res*. 1992;70:1122–1127.
26. Kacem K, Seylaz J, Issertial O, Aubineau P. Chemical sympathectomy favours vimentin expression in arterial smooth muscle cells of young rats. *J Auton Nerv Syst*. 1995;53:57–68.
27. Damon DH. NGF-independent survival of postganglionic sympathetic neurons in neuronal-vascular smooth muscle cocultures. *Am J Physiol Heart Circ Physiol*. 2001;280:H1722–H728.
28. Cowen T, Gavazzi I. Plasticity in adult and ageing sympathetic neurons. *Prog Neurobiol*. 1998;54:249–288.
29. Cao L, Jiao X, Zuzga DS, Liu Y, Fong DM, Young D, During MJ. VEGF links hippocampal activity with neurogenesis, learning and memory. *Nat Genet*. 2004;36:827–835.
30. Zimmerman GC, Keeling JH, Lowry M, Medina J, Von Hoff DD, Burris HA. Prevention of docetaxel-induced erythrodysesthesia with local hypothermia. *J Natl Cancer Inst*. 1994;86:557–558.

CLINICAL PERSPECTIVE

Vascular endothelial growth factor (VEGF) is a key angiogenic factor, and blocking of VEGF signaling in cancer patients inhibits angiogenesis, thereby preventing tumor progression. One of the side effects of anti-VEGF therapy is the hand-foot syndrome, which is characterized by dilated blood vessels in hands and feet, leading to dysesthesia, erythema, and tingling of extremities, which may progress to burning pain with dryness, cracking, and ulceration of the skin. Here, we show that knock-in mice with reduced VEGF levels display abnormal regulation of resistance arteries, resulting in defects in thermoregulation and redistribution of blood flow in response to hypoxia. The abnormal vascular regulation was attributed to reduced vascular smooth muscle cell contractility associated with reduced expression of contractile proteins, as well as to dysfunction of neuroeffector junctions as a result of their abnormal structural development. Furthermore, short-term treatment of wild-type mice with a VEGF trap also induced thermoregulation defects and neuroeffector dysfunction with structural remodeling of neuroeffector junctions, indicating that VEGF is necessary for maintenance of the structural and functional integrity of adult neuroeffector junctions. These findings may provide mechanistic insights into the cause of the hand-foot syndrome.

SUPPLEMENTAL MATERIAL

SUPPLEMENTAL METHODS

Histology and immunohistochemistry: For whole mount staining of arteries, first order mesenteric and saphenous arteries were dissected and fixed in 80% MeOH/20% DMSO (TH staining) or in 1%PFA (VEGFR stainings) at 4°C overnight. TH staining: after rehydration and blocking with 2% TBS-BSA, vessels were incubated with a rabbit anti-TH antibody (Chemicon; 1:100) overnight. Finally, incubation with an Alexa488-labeled goat anti-rabbit IgG (1/200) was performed. VEGFRs staining: arteries where permeabilized with 0.05% Triton X-100 in PBS, blocked with 5% goat pre-immune serum and incubated overnight at 4°C with antibodies against Flt1 (5µg/ml, SC-316) or Flk1 (5µg/ml, SC-504). Finally, 1h incubation with Alexa-labeled secondary antibodies was performed. Vessels were mounted on glass slides and 3D images were obtained with a Zeiss LSM510 confocal laser scanning microscope and analyzed with Zeiss KS300 software. For analysis of skin vascular density, ears from 1 month old mice were dissected as described [1]. The ears were fixed in ice cold Dent's fixative overnight and blocked with 2% TBS-BSA. For whole mount double immunostaining the tissues were incubated with anti-SM alpha-actin (Dako, 1/500) and anti-CD31 (Pharmingen, 1/500) followed by incubation with Alexa-labeled secondary antibodies and flat-mounting.

LacZ enzymatic staining was performed on 20 µm transverse cryo-sections of unfixed saphenous and mesenteric arteries. After fixation in acetone for 20 min at -20°C, slides were washed in washing buffer (0.1% Sodium deoxycholate, 0.2% Nonidet P40 and 2mM $MgCl_2$ in PBS) and incubated overnight at 30°C in X-gal staining solution (2mM

MgCl$_2$, 5 mM K$_4$Fe(CN)$_6$, 5 mM K$_3$Fe(CN)$_6$ and 1mg/ml X-gal in PBS). Afterwards slides were washed in PBS, counterstained with nuclear fast red and mounted with mowiol (Sigma). For alkaline phosphatase (AP) binding and staining, VEGF-B^{186}-AP and VEGF^{164}-AP (VEGF-AP) fusion proteins were made by cloning VEGF-B^{186} or VEGF^{164} cDNA in a pAPtag-5 vector (GenHunter). Fusion proteins were then expressed in HEK-293 cells as secreted protein, and the conditioned medium was used directly as a highly sensitive affinity agent. AP activity was tested via an AP-activity assay and the AP binding assay was performed as previously described [2]. Imaging analysis was performed on a Zeiss Axioplan2 connected to a 3CCD video camera (DXC-93OP, Sony), and KS300 software (Zeiss, Germany). For the anaylsis of SMC differentiation markers and VEGF expression on saphenous and mesenteric arteries, arteries were dissected, fixed in 1%PFA (4ºC, overnight), cryo-protected and cryo-sectioned. Immunostainings were performed with the following antibodies: anti-smoothelin (1:100, gift of G. van Eys, Maastricht University), anti-SM myosin HC (1:400, ab683, Abcam), anti-desmin (1:50, 10519, Cappel) and anti-VEGF (1/50, SC152G), followed by 2h incubation with Alexa-labeled secondary antibodies. For measurement of relative fluorescence intensity, arteries from VEGF$^{\partial/\partial}$ and control mice were harvested and stained simultaneously, and images were acquired in random order in a single session. Fluorescence intensity was measured using Zeiss KS300 software with subtraction of background fluorescence.

Noradrenaline content: Saphenous and mesenteric resistance artery segments, kidney and heart were solubilized in 0.5 M acetic acid (15 minutes, 100°C). Noradrenaline content of the extract was measured by high-performance liquid chromatography and fluorescent detection, after which the tissues were solubilized in 1N KOH (24 hours, room

temperature) and DNA content was determined. Noradrenaline levels were expressed relative to DNA content.

Murine VEGF ELISA: For quantification of mVEGF protein expression, the Mouse VEGF Quantikine ELISA Kit (R&D Systems) was used. mVEGF concentrations were normalized to total protein concentration, which was measured using BCA assay (Pierce).

Isometric wire myography: Two-millimeter segments of isolated first order mesenteric, saphenous and common carotid arteries were mounted (steel wires, diameter 40 μm) in a myograph organ bath (model 610, Danish Myotechnology by J.P. Trading, Denmark) for isometric force measurements. Organ baths were filled with a Krebs-Ringer bicarbonate buffer, maintained at 37°C, and aerated with 95% O_2 and 5% CO_2. Each individual arterial segment was distended to a diameter at which a maximal contractile response to 10 μM NA could be obtained. To evaluate SMC function, the following stimuli were used: (i) concentration-response curve for increasing concentrations of extracellular K^+ (in exchange for Na^+), (ii) concentration-response curve for angiotensin II (1-30 nM) during mild depolarization (16.5-25 mM K^+), (iii) concentration-response curve for NA (0.01-10 μM), (iv) concentration-response curve for the thromboxane A_2-analogue U46619 (1-100 nM), (v) concentration-response curve for U46619 in the continuous presence of the NO-synthase inhibitor nitro-L-arginine (NLA, 30μM). Endothelium-dependent relaxing responses to acetylcholine were evaluated during contractions induced by 40 mM K^+, 10 μM NA and 100 nM U46619 and the relaxing effects of the NO-donor substance Sodium nitroprusside (SNP, 0.01 to 10 μM) were studied during contraction induced by U46619, in the presence of the NO-synthase inhibitor NLA. To evaluate perivascular sympathetic nerve function, the following stimuli were used: (i) response to increasing frequencies

3

(0.25-32 Hz) of electrical field stimulation (EFS) delivered by two platinum electrodes placed along the isolated arterial segment, (ii) concentration-response curve for increasing concentrations (1-100 μM) of tyramine, (iii) effect of cocaine on the arterial sensitivity to increasing concentrations (0.01-10 μM) of exogenous NA, (iv) addition of the alpha-adrenoreceptor antagonist phentolamine (1 μM) on top of a maximal contractile response to 125 mM K^+. To evaluate perivascular sensory-motor nerve function, mesenteric arteries were induced to contract by U46619 (0.1 μM), and the relaxing effect of either capsaicin (0.1 and 1.0 μM, a compound that stimulates the release of endogenous CGRP from sensory-motor nerves [3, 4]) or exogenous CGRP (0.1 to 300 nM) was evaluated. At the end of the experiments, vessel segments were fixed in the organ chamber in phosphate-buffered formaldehyde (4%, pH 7.4, 37°C, 30 minutes) for subsequent morphometric analysis.

Glyoxylic acid staining: Glyoxylic acid was used to visualize and quantify perivascular sympathetic nerve fibers in whole mount preparations of isolated first order mesenteric and saphenous arteries. Vessels were mounted and stretched in an organ bath (see above) and incubated in 2% glyoxylic acid and 10% sucrose in phosphate buffer for 10 minutes at room temperature. Segments were then air dried (90 sec), stretched at 100°C for 4 minutes and mounted on glass slides. Two-photon laser scanning microscopy was used to generate a stack of images from one side of the compressed vessels[3, 4]. The percentage of the area occupied by fluorescent signal was calculated.

Noradrenaline reuptake experiments: Mesenteric and saphenous arteries were dissected and the length of the arterial segments was determined. Pre-incubation, incubation and wash steps were done in Krebs Ringer bicarbonate solution containing EGTA (1 mM) and glutathione (10 mM) (=KRB^+ buffer), either in the absence or the

presence of 3 µM cocaine, an established inhibitor of NA neuronal uptake. After pre-incubation (37°C, 30 min), 0.1 µM levo-[ring-2,5,6-^{3}H]-NA (52.6 Ci/mmol, Perkin Elmer) was added to the KRB$^+$ buffer (incubation at 37°C for 60 min). During the wash step (37°C, 60 min), arteries were transferred repeatedly (10 times) to fresh KRB$^+$. For extraction of the ^{3}H-NA, arteries were transferred to 1 ml of 0.5 M acetic acid containing 10 mM glutathione, and heated at 94°C during 15 minutes. Subsequently, the artery was recovered and digested in 100 µl 1N KOH during 48 hours, followed by DNA content determination. The extract was used for liquid scintillation spectrometry. Liquid scintillation results (in CPM) were normalized to vessel segment length or to DNA content, and the difference between findings obtained in the absence and presence of cocaine was used as a measure of NA reuptake capacity.

Transmission electron microscopy: Mice were anesthetized, perfused with 4% PFA and 2.5% glutaraldehyde in Na-cacodylate buffer (0.1 M), pH 7.3 for 15 minutes. Two saphenous and three second order mesenteric resistance arteries were dissected from each mouse and fixed overnight in 4%PFA and 2.5% glutaraldehyde in Na-cacodylate buffer (0.1 M). The next day two rinses (2 x 30 min) with Na-cacodylate buffer (0.1 M) were followed by postfixation with 2% osmiumtetroxide in Na-cacodylate buffer (0.1 M) for 2h at room temperature. Following dehydration in a graded ethanol series (30-50-70%, each step 2 x 15 min) the arteries were block stained with 1% uranylacetate in 70% ethanol for 30 min at room temperature. After the last steps of the dehydration (96-100%, each step 2 x 15 min) the impregnation of the tissue with freshly prepared Agar 100 (EPON 812, Medium) was initiated by means of a graded propylene oxide – Agar 100 series (100% propylene oxide, 2 x 20 min – propylene oxide 1:1 Agar 100, 1 hour – propylene oxide 1:2 Agar 100, overnight in a dessicator, room temperature). The next day the arteries were

5

transferred to freshly prepared Agar 100 and placed in a dessicator for 6 to 8 hours at room temperature before they were orientated in molds and put in an oven at 60° C for 48 hours for the polymerization of the resin. Semi thin (0.5-1 μm) sections were made and stained with 1% toluidine blue in 1% borax for light microscopic observations. Ultra thin sections (70 nm) were placed on copper grids (400 mesh) and contrasted with 4% uranyl acetate for 10 min and lead citrate for 5 min. Ultrastructural observations were made with a JEOL JEM 2100 at 200 kV at the KULeuven Electron Microscopy Core Facility of the Department of Human Genetics, Leuven, Belgium. Light microscopic and ultrastructural observations were quantitatively analyzed using Zeiss KS 300 3.0 software.

For morphometric analysis, high power electron micrographs were made of neuro-effector junctions in randomly selected single sections and used to measure (i) the shortest distance between nerve varicosities and the nearest vascular SMCs, as described [5] (ii) the average number of mitochondria per varicosity, (iii) the surface area of varicosities, (iv) the number of varicosities per axon bundle, and (v) the density of transmitter storage vesicles (number per varicosity/surface area varicosity), as described [6]. Image acquisition and morphometric analysis of electron micrographs were performed by an investigator blinded to the mouse genotype.

Blood flow measurements: Magnetic resonance (MR) experiments were performed on a 7T horizontal bore magnet and 8-cm aperture self-shielded gradients with a maximum strength of 0.1 T/m (Oxford Instrument, UK) equipped with a MRRS console (MRRS, UK). Mice were anesthetized using 5% isoflurane for induction and a maintenance dose of 0.4%-0.8% isoflurane in a mixture of O_2:N_2O (3:7) at a flow rate of 600 ml/min. Refined monitoring systems recorded body temperature (Kent, UK), breaths per minute and end-

tidal CO_2 (Capstar-100, Linton Instruments, UK), which were, respectively, 37.0 ± 0.2°C, 180 ± 20 and 3.5 ± 0.5%.

Arterial Spin Labeling: Continuous Arterial Spin Labeling (ASL) was used to study the response of CBF to hypoxia (200s at 8%O2). Single slice EPI-GE paired images were acquired alternately: one without arterial labelling (control image) and the other with arterial labelling. For each set of CBF measurements, 150 pairs of images were acquired and the first 4 pairs were discarded. All mice were spontaneously breathing and during ASL acquisition, ventilation parameters were set to hypoxic conditions by switching from 30% O_2 to 8% O_2. One trial per mouse consisted of 80 ASL measurements during normoxia, followed by 40 measurements during hypoxia after which recovery was allowed during 30 measurements. Arterial spin labelling signal changes were analysed using home written programs in IDL (Boulder, UK), which provide regional analyses on a pixel per pixel base. The most straightforward approach of "simple subtraction" was used, which means direct pairwise subtraction between temporally adjacent label and control acquisitions. Analysis of the percent changes reveals whether the hypoxia induced CBF increase is present without the need to calculate the absolute CBF in ml/g/min.

Purification and culture of SCG and CG neurons: SCGs and CGs from WT or VEGF$^{\partial/\partial}$ P4 pups were dissected and placed in 0.25% trypsin-EDTA (Invitrogen) for 30min at 37ºC, washed twice with Hank's buffered salt solution (HBSS) containing Ca^{2+} and Mg^{2+} (Invitrogen) and then placed in 1x collagenase in HBSS with Ca^{2+} and Mg^{2+} for 30min and 37ºC. Ganglia were then dissociated by trituration. Neurons were finally resuspended and cultured in Neurobasal medium (Gibco) containing B27 (Gibco) on poly-L and laminin coated coverslips for 48h.

Table S1: Structural vessel parameters

Artery	Parameter	WT	VEGF$^{a/a}$
Mesenteric	Lumen diameter	166 ± 11	146 ± 17
	Media area	2,260 ± 193	1,480 ± 258*
	Media thickness	5.1 ± 0.6	3.1 ± 0.2*
Saphenous	Lumen diameter	221 ± 6	159 ± 6*
	Media area	6,385 ± 460	3,720 ± 610*
	Media thickness	8.7 ± 0.5	8.9 ± 1.0
Carotid	Lumen diameter	385 ± 20	356 ± 20
	Media area	18,400 ± 700	15,400 ± 1,000
	Media thickness	14.8 ± 0.4	13.3 ± 0.6

The data represent the mean ± SEM of 5-11 measurements of the diameter of the lumen (μm), cross-sectional area of the media (μm^2), and thickness of the media (μm). *: $p < 0.05$ versus WT.

8

Table S2: Maximal contractile responses of resistance and elastic arteries

Artery	Stimulus	Tension *Stress*	WT	VEGF$^{\partial/\partial}$
Mesenteric	K$^+$	N/m	0.88 ± 0.11	0.14 ± 0.04*
		N/m^2	*172 ± 35*	*45 ± 15**
	Ang II	N/m	0.73 ± 0.04	0.12 ± 0.05*
		N/m^2	*143 ± 46*	*38 ± 19**
	NA	N/m	1.41 ± 0.13	0.31 ± 0.09*
		N/m^2	*276 ± 40*	*100 ± 32**
	U46619	N/m	1.28 ± 0.16	0.29 ± 0.11*
		N/m^2	*251 ± 54*	*97 ± 46**
Saphenous	K$^+$	N/m	2.91 ± 0.31	0.94 ± 0.54*
		N/m^2	*323 ± 46*	*105 ± 35**
	NA	N/m	2.92 ± 0.28	0.96 ± 0.44*
		N/m^2	*327 ± 44*	*131 ± 49**
	U46619	N/m	2.57 ± 0.22	0.79 ± 0.42*
		N/m^2	*289 ± 45*	*110 ± 52**
Carotid	K$^+$	N/m	0.58 ± 0.11	0.52 ± 0.11
		N/m^2	*40 ± 7*	*39 ± 9*
	NA	N/m	0.65 ± 0.08	0.49 ± 0.09
		N/m^2	*45 ± 6*	*36 ± 6*
	U46619	N/m	1.04 ± 0.03	1.29 ± 0.28
		N/m^2	*100 ± 11*	*97 ± 22*

The data represent the mean ± SEM of 5-11 measurements of the maximal active wall tension (N/m) and wall stress (N/m^2) in response to potassium (K$^+$), angiotensin II (Ang II), NA (NA) or the thromboxane agonist (U46619). *: p < 0.05 versus WT.

Table S3: Tissue NA content

Parameter	Tissue	WT	VEGF$^{\partial/\partial}$
	heart	447 ± 69	455 ± 41
NA content	kidney	86.6 ± 7.3	128.2 ± 17.1
(pg NA/µg DNA)	mesenteric artery	2,970 ± 821	4,840 ± 472
	saphenous artery	2,720 ± 690	1,890 ± 147

The values represent the mean ± SEM of 6 measurements of the noradrenaline (NA) content of 3 month old mice.

Table S4: Blood pressure and heart rate of VEGF$^{\partial/\partial}$ and WT control mice.

Parameter	WT	VEGF$^{\partial/\partial}$
systolic BP (mmHg)	94.6 ± 9.8	90.6 ± 4.0
diastolic BP (mmHg)	59.7 ± 9.2	68.1 ± 4.4
MAP (mmHg)	75.7 ± 9.9	78.9 ± 4.5
heart rate (bpm)	500 ± 25	491 ± 30

The values represent the mean ± SEM of 5 measurements. BP: blood pressure; MAP: mean arterial blood pressure; bpm: beats per minute. At first sight, one might expect that an impairment in vasoconstrictor response, as observed in VEGF$^{\partial/\partial}$ mice, would automatically result in hypotension. However, the regulation of blood pressure is a complex process, involving the interplay of numerous molecules. Several gene-inactivation studies in mice indicate that loss of even key players of vascular regulation fail to significantly affect the blood pressure in baseline conditions, presumably because of compensatory up- or downregulation of additional vasoactive substances [7-13]. Alternatively, the defect in vascular regulation in the VEGF$^{\partial/\partial}$ mice may be too subtle to influence homeostasis in baseline conditions, but sufficient to be relevant in stress conditions.

Table S5: Relative expression levels of smooth muscle cell differentiation markers in sFlk1 and control mice.

Artery	target gene	Control	sFlk1	p-value
Saphenous artery	SM myosin heavy chain	100 ± 9.6	114.3 ± 13.7	0.40
	smoothelin	100 ± 7.9	105.8 ± 9.8	0.65
Mesenteric artery	SM myosin heavy chain	100 ± 13.7	132.9 ± 30.3	0.33
	smoothelin	100 ± 12.5	81.4 ± 11.7	0.30
Carotid artery[A]	SM myosin heavy chain	100 ± 70.3	106.7 ± 48.2	0.94
	smoothelin	100 ± 70.0	154.9 ± 69.0	0.58

Relative expression levels as percentage of WT ± SEM are shown. [A] Common carotid arteries were used.

TableS6: Ultrastructural parameters of perivascular neuro-effector junctions of sFlk1 and control treated mice.

Artery	Parameter	Control	sFlk1
Mesenteric	junctional cleft width	0.85 ± 0.02	1.48 ± 0.04*
	number of mitochondria/varicosity	2.62 ± 0.29	2.75 ± 0.30
	varicosity area	0.87 ± 0.09	0.87 ± 0.11
	number of varicosities/axon bundle	3.45 ± 0.24	2.67 ± 0.24*

The data represent the mean ± SEM of measurements of the distance between nerve varicosities and SMCs (junctional cleft width in μm), the number of mitochondria per varicosity, varicosity area ($μm^2$) and number of varicosities per axon bundle. *: $p < 0.05$

SUPPLEMENTAL NOTES

Note S1: VEGF protein levels in peripheral resistance arteries: pg VEGF/mg total protein: for saphenous arteries: 65.8±11.5 in WT mice versus 43.5±5.8 in VEGF$^{\partial/\partial}$ mice; n=8; p=0.03; for mesenteric arteries: 126.3±11.3 in WT mice versus 94.8±8.2 in VEGF$^{\partial/\partial}$ mice; n=8; p=0.04. VEGF protein levels in superior cervical ganglia: pg VEGF/mg total protein: medians (interquartile range): 96.6 (82.1-102.8) in WT mice versus 68.5 (67.1-75.0) in VEGF$^{\partial/\partial}$ mice; n=8-10; Mann Whitney p-value=0.002. To ensure that these ELISA measurements reflected reduced VEGF expression in postganglionic neurons, ganglia were dissociated and neurons were cultured for 48h, followed by RNA isolation. Quantitative real-time PCR revealed reduced VEGF expression in VEGF$^{\partial/\partial}$ neurons (relative VEGF expression: medians (interquartile range): 2.05 (1.30-2.65) in VEGF$^{\partial/\partial}$ neurons versus 3.10 (2.35-3.35) in WT neurons, n=10-13; Mann Whitney p-value=0.015).

Note S2: To analyze whether noradrenaline (NA) reuptake by perivascular nerves was normal, mesenteric and saphenous arteries of 2 month old VEGF$^{\partial/\partial}$ mice were dissected and incubated with ^{3}H-labeled NA in the presence or absence of the NA reuptake inhibitor cocaine. The NA reuptake capacity was then calculated as the difference between the condition with and without cocaine (see Methods for details). This approach failed to reveal defects in NA reuptake in mesenteric arteries of VEGF$^{\partial/\partial}$ mice (NA reuptake in cpm/mg DNA: 431 ± 104 in VEGF$^{\partial/\partial}$ mice versus 485 ± 98 in WT mice; n=10, p=0.72), as well as in saphenous arteries (NA reuptake in cpm/mg DNA: 407 ± 113 in VEGF$^{\partial/\partial}$ mice versus 419 ± 89 in WT mice; n=6, p=0.93). Thus, alteration of NA reuptake by perivascular nerves could not explain the autonomic defects in VEGF$^{\partial/\partial}$ mice.

Note S3: Thyroid function was evaluated by measuring plasma T3 and T4 hormone levels. No differences were found between WT and VEGF$^{\partial/\partial}$ mice (T3 levels in ng/dl: 58.3 ± 0.88 versus 55.3 ± 2.7 respectively in WT and VEGF$^{\partial/\partial}$ mice, n=3, p=0.35; T4 levels in µg/dl: 4.63 ± 0.71 versus 3.03 ± 0.29 respectively in WT and VEGF$^{\partial/\partial}$ mice, n=3, p=0.11).

Note S4: µg Flk1/mg protein: in mesenteric arteries: 0.24±0.08 for control versus 0.84±0.07 for sFlk1, n=5, p=0.0005; in saphenous arteries: 0.67±0.11 for control versus 3.21±1.08 for sFlk1, n=5, p=0.04.
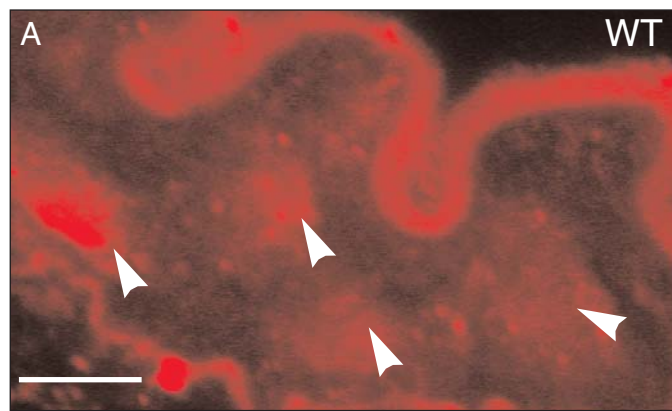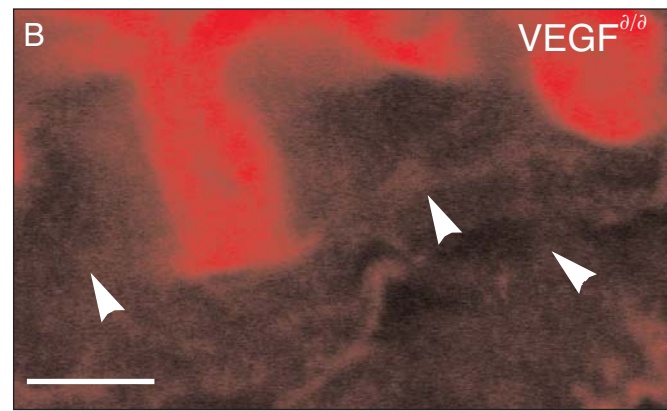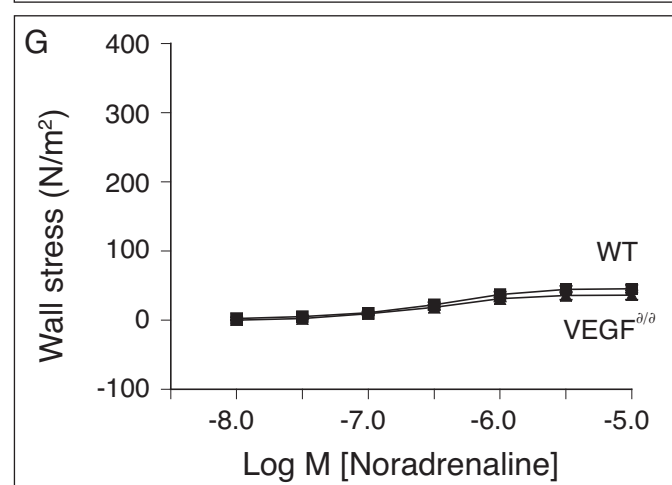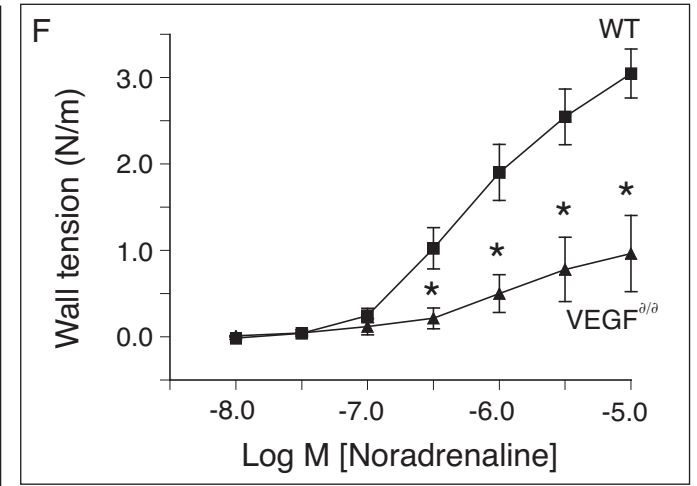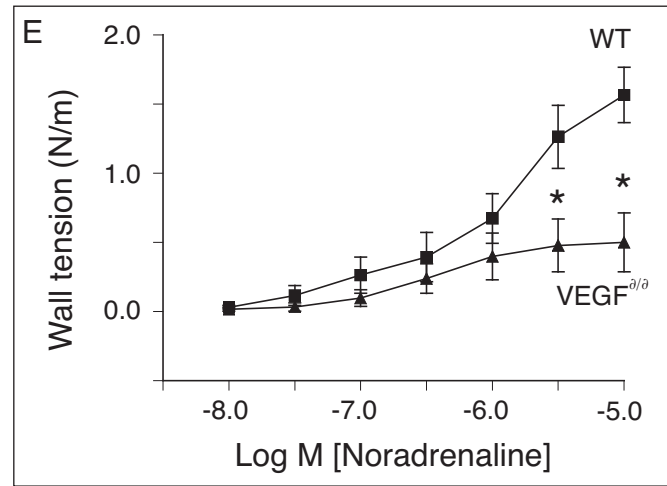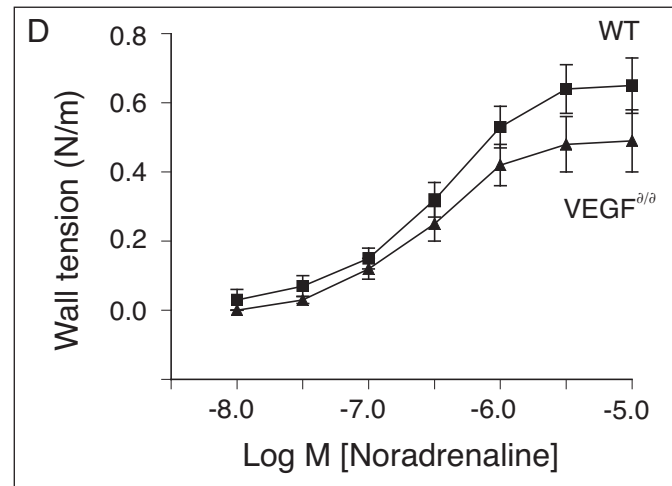
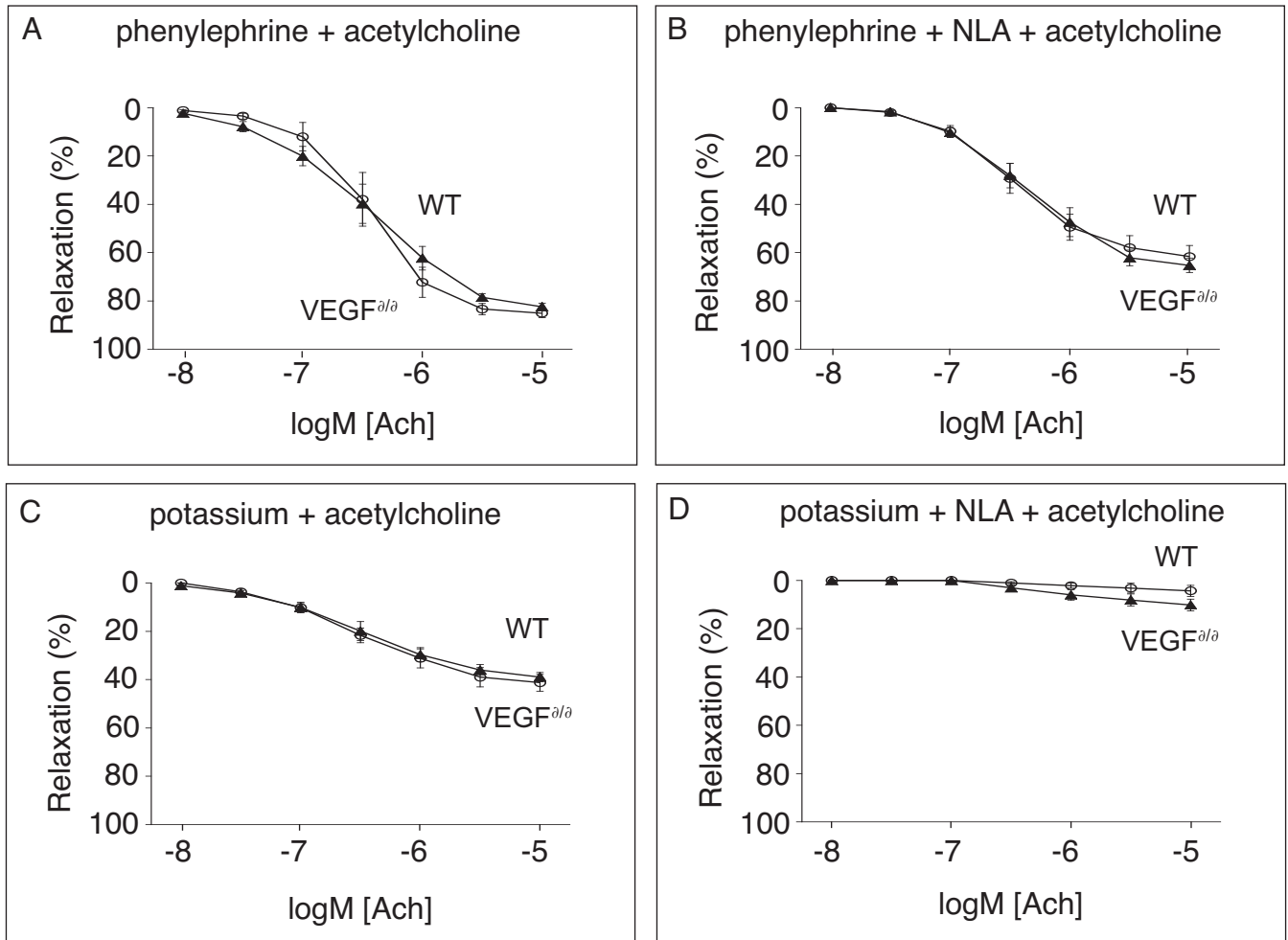**Carotid Artery** **Mesenteric Artery** **Saphenous Artery**
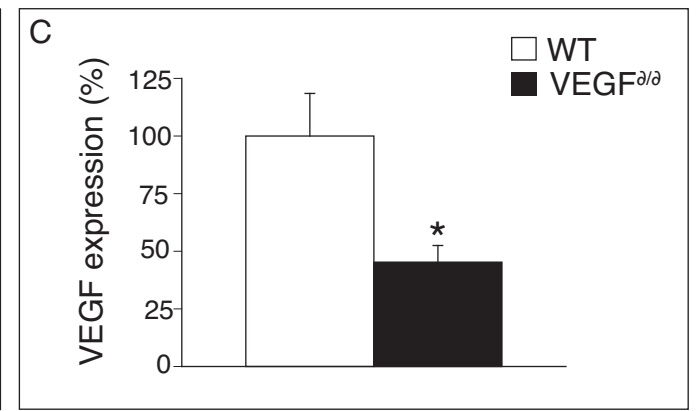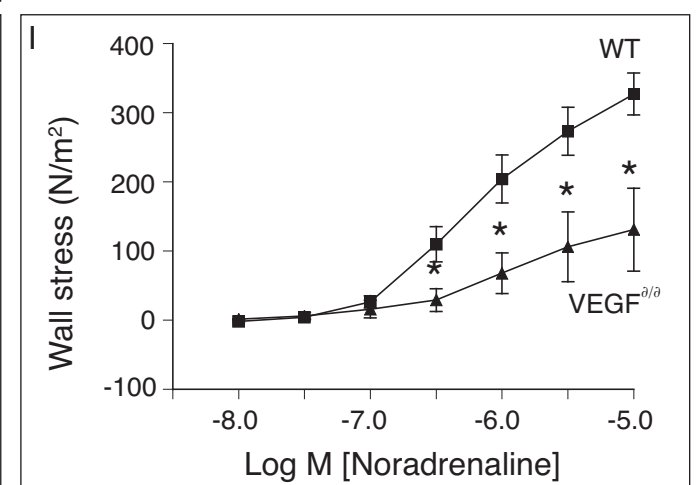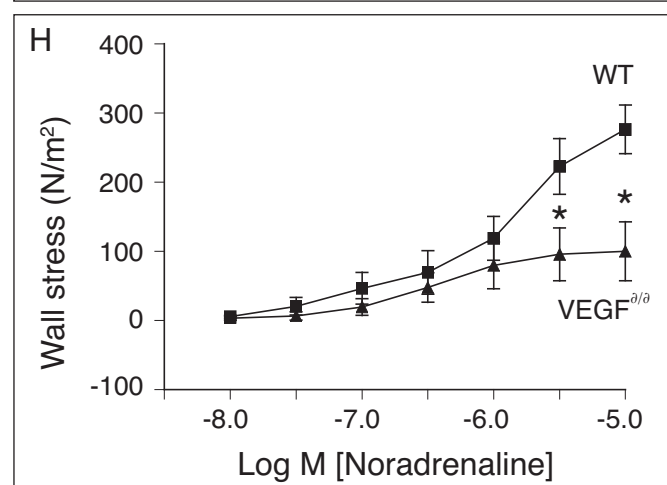
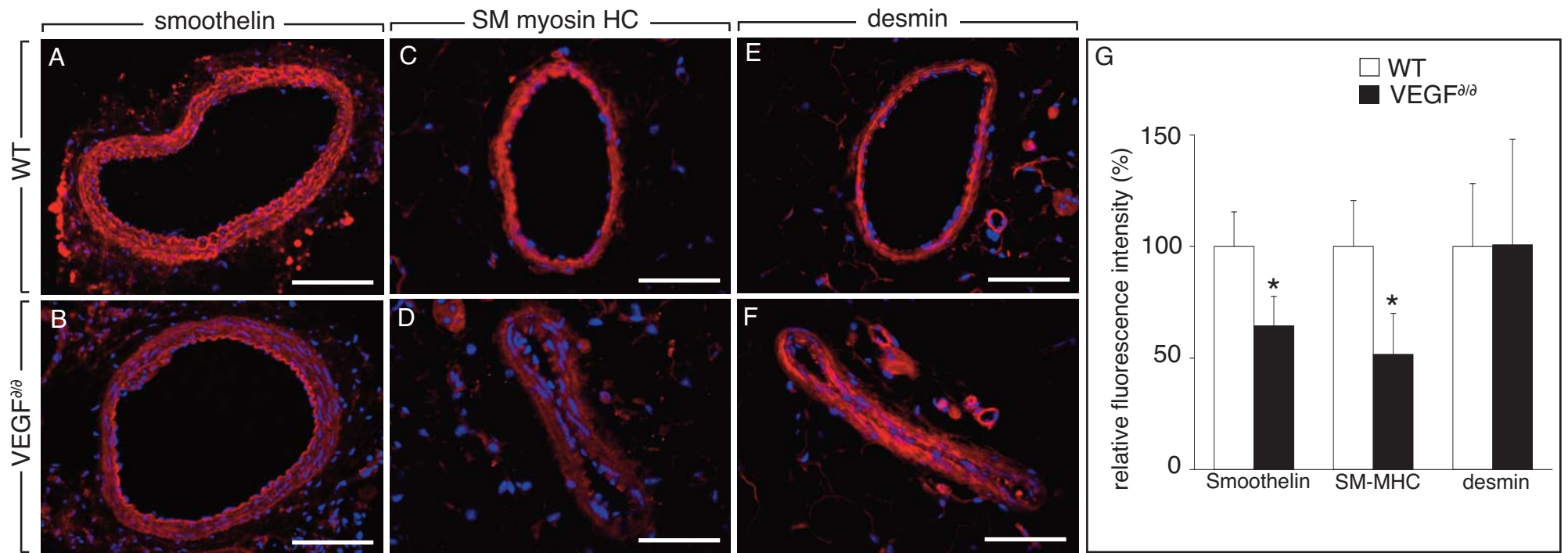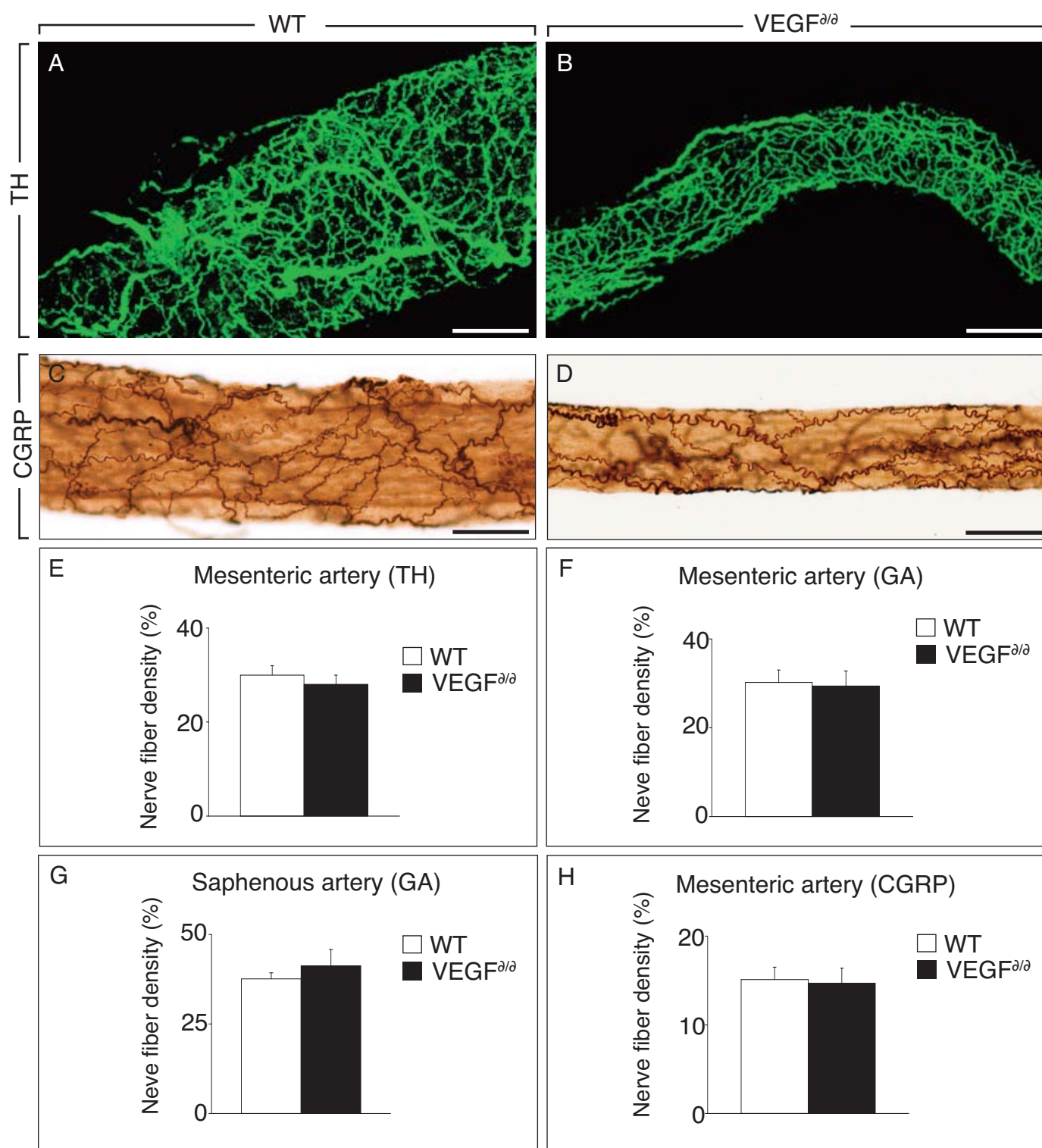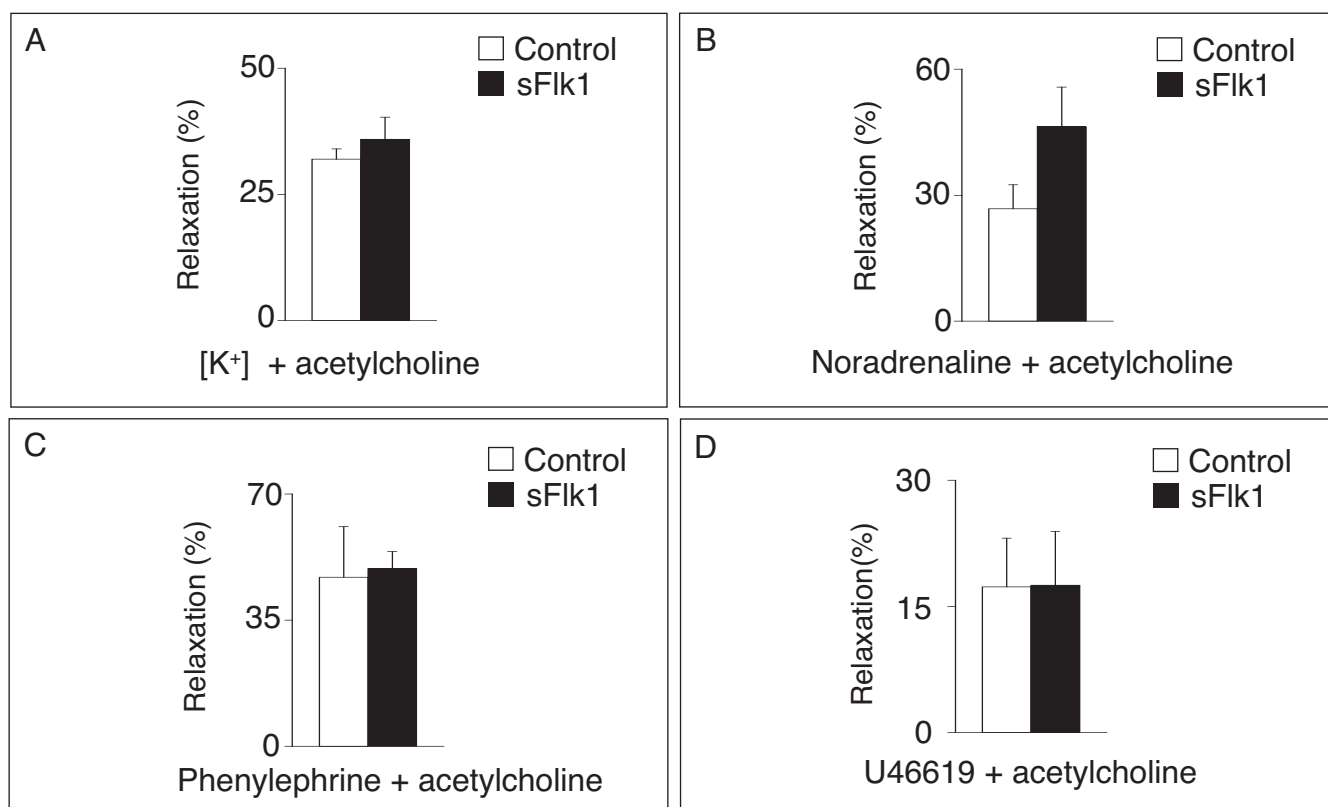**Figure S1**

Figure S2

Figure S3

Figure S4

Figure S5

SUPPLEMENTAL FIGURE LEGENDS

Figure S1: Reduced VEGF expression and vascular SMC dysfunction in peripheral resistance arteries of VEGF$^{\partial/\partial}$ mice. **A-B,** Representative pictures of VEGF immunostaining on mesenteric arteries from WT (*A*) and VEGF$^{\partial/\partial}$ mice (*B*) showing a reduced VEGF staining intensity in VEGF$^{\partial/\partial}$ arteries compared to WT. Scale bar: 5μm. **C,** Relative intensity of VEGF immunostaining in the SMC layer of mesenteric arteries, displayed as % of WT (* P=0.029, N=4). **D-F**, Concentration response curveof carotid arteries *(D)*, mesenteric arteries *(E)* and saphenous arteries *(F)* of WT and VEGF$^{\partial/\partial}$ mice in response to NA. Vasoconstriction is significantly reduced in mesenteric and saphenous resistance arteries of VEGF$^{\partial/\partial}$ mice, but normal in carotid arteries. **G-I,** Even when the size of the vessels was taken into account (active wall stress), VEGF$^{\partial/\partial}$ mesenteric and saphenous arteries exhibited a marked reduction in contractility, whereas contractility of carotid arteries was normal. Note that in WT mice active wall stress was markedly larger in the muscular mesenteric and saphenous arteries than in the elastic carotid artery, and that this regional difference was largely abolished in VEGF$^{\partial/\partial}$ mice. *: $p < 0.05$ versus WT.

Figure S2: Normal endothelial function in VEGF$^{\partial/\partial}$ resistance arteries. To analyze the role of the endothelium in vascular regulation, we studied the response to acetylcholine (Ach), which relaxes arterial smooth muscle by inducing the release of endothelium-derived factors. In isolated mesenteric arteries, relaxing responses to increasing concentrations of acetylcholine were recorded during contraction induced by 20 μM phenylephrine *(A,B)* or high potassium (40 mM K$^+$) *(C,D)*, in the absence *(A,C)* or the presence *(B,D)* of the NO-synthase inhibitor

16

nitro-L-arginine (NLA, 30 µM). Regardless of the vasoconstrictor, a dose range of 0.01 to 10 µM Ach induced comparable relaxations in VEGF$^{\partial/\partial}$ and control arteries, indicating that vascular regulation by ECs was normal in VEGF$^{\partial/\partial}$ mice.

Figure S3: Reduced expression of late vascular SMC differentiation markers in VEGF$^{\partial/\partial}$ arteries. *A-F,* Representative pictures of immunostaining for smoothelin *(A, B)*, smooth muscle myosin heavy chain *(C, D)* and desmin *(E, F)* on saphenous arteries of WT (upper panels: *A, C, E*) and VEGF$^{\partial/\partial}$ mice (lower panels: *B, D, F*). Staining intensity is reduced in VEGF$^{\partial/\partial}$ arteries for smoothelin and smooth muscle myosin heavy chain, but not for desmin. Scale bar: 50µm. *G,* Relative intensity of immunostaining in the tunica media of saphenous arteries, displayed as % of WT. *: $p < 0.05$ versus WT.

Figure S4: Neuro-effector dysfunction cannot be attributed to reduced density of peri-arterial nerves. To examine whether the reduced response of muscular arteries to neurogenic stimuli in VEGF$^{\partial/\partial}$ mice was due to a reduced density of sympathetic innervation (caused by a developmental defect at 3 weeks of age, or by nerve degeneration at the age of 3, 6 and 12 months), we stained whole-mount mesenteric arteries for tyrosine hydroxylase (TH), a marker of the perivascular sympathetic plexus. Light microscopic analysis of these whole mount stained vessels only allows one to visualize axon bundles of the autonomic plexus, but not the more subtle ultrastructural changes that can be observed by EM. (i) At 3 WEEKS OF AGE (i.e. after the sympathetic plexus is formed), a dense network of strongly stained interconnecting fibers was detectable over the entire surface of these vessels in both genotypes. Quantification of the TH-immunoreactive area as a percentage of the total vessel area revealed that the TH$^+$ nervous plexus covered a similar vessel area in both

genotypes at 3 weeks of age (30 ± 2% in WT mice versus 28 ± 2% in VEGF$^{\partial/\partial}$ mice; n=6-11, p=0.45; Figure S4A,B,E; scale bar: 25 μm), indicating that development of the perivascular adrenergic plexus was normal. (ii) By 3 MONTHS OF AGE, when vasoregulator control by perivascular nerves was dysfunctional in VEGF$^{\partial/\partial}$ mice, the TH$^+$ nervous plexus comprised 21 ± 1% in WT mice versus 27 ± 2% in VEGF$^{\partial/\partial}$ mice (n=6-9, p=0.07). Similar findings were observed when analyzing the density of nerve fibers by staining with glyoxylic acid (Figure S4F,G). We also stained transverse sections of saphenous arteries for TH. Again, quantification revealed no genotypic differences in the density of perivascular nerves (number of perivascular nerves per section, respectively, for WT and VEGF$^{\partial/\partial}$: 25.1 ± 4.6 versus 19.6 ± 2.6, n=10-14, p=0.75). Likewise, sensory-motor nerve dysfunction could not be attributed to nerve degeneration as the density of CGRP-immunoreactive nerve fibers in whole mount mesenteric artery preparations did not significantly differ between WT and VEGF$^{\partial/\partial}$ (15.1 ± 1.4% in WT mice versus 14.7 ± 1.7% in VEGF$^{\partial/\partial}$ mice; n=8, p=0.35; Figure S4C,D,H; scale bar: 25μm). (iii) Also, BY 6 MONTHS OF AGE, when VEGF$^{\partial/\partial}$ mice exhibit the first symptoms of motor neuron degeneration, no perivascular sympathetic nerve degeneration could be observed, as the TH$^+$ nervous plexus comprised 28 ± 3% in WT mice and 29 ± 3% in VEGF$^{\partial/\partial}$ mice (n=5-8, p=0.77). (iv) Even IN AGED, 1 YEAR OLD VEGF$^{\partial/\partial}$ mice, the sympathetic nervous plexus was intact (24 ± 3% in WT mice versus 28 ± 3% in VEGF$^{\partial/\partial}$ mice: n=6, p=0.21). Thus, perivascular nerve terminals are dysfunctional in VEGF$^{\partial/\partial}$ mice, but do not show obvious signs of nerve degeneration, at least not at the light-microscopical level.

Figure S5: Reduction of VEGF plasma levels in WT mice by sFlk1 does not impair endothelial cell function. *A-D,* Vasodilator response to acetylcholine (10

μM) during contraction induced by high potassium (40 mM) *(A)*, NA (10 μM) *(B)*,

phenylephrine (10 μM) *(C)* and U46619 (100 nM) *(D)*.

19

SUPPLEMENTAL REFERENCES

1. Makinen T, Adams RH, Bailey J, Lu Q, Ziemiecki A, Alitalo K, Klein R, Wilkinson GA. PDZ interaction site in ephrinB2 is required for the remodeling of lymphatic vasculature. *Genes Dev.* 2005;19:397-410.

2. Flanagan JG, Cheng HJ, Feldheim DA, Hattori M, Lu Q, Vanderhaeghen P. Alkaline phosphatase fusions of ligands or receptors as in situ probes for staining of cells, tissues, and embryos. *Methods Enzymol.* 2000;327:19-35.

3. De Mey JG, Megens R, Fazzi GE. Functional antagonism between endogenous neuropeptide Y and calcitonin gene-related peptide in mesenteric resistance arteries. *J Pharmacol Exp Ther.* 2008;324:930-937.

4. Meens MJ, Fazzi GE, van Zandvoort MA, De Mey JG. Calcitonin gene-related peptide selectively relaxes contractile responses to endothelin-1 in rat mesenteric resistance arteries. *J Pharmacol Exp Ther.* 2009;331:87-95.

5. Luff SE, Young SB, McLachlan EM. Hyperinnervation of mesenteric arteries in spontaneously hypertensive rats by sympathetic but not primary afferent axons. *J Vasc Res.* 2005;42:348-358.

6. Verstreken P, Ohyama T, Haueter C, Habets RL, Lin YQ, Swan LE, Ly CV, Venken KJ, De Camilli P, Bellen HJ. Tweek, an evolutionarily conserved protein, is required for synaptic vesicle recycling. *Neuron.* 2009;63:203-215.

7. Altman JD, Trendelenburg AU, MacMillan L, Bernstein D, Limbird L, Starke K, Kobilka BK, Hein L. Abnormal regulation of the sympathetic nervous system in alpha2A-adrenergic receptor knockout mice. *Mol Pharmacol.* 1999;56:154-161.

8. Chruscinski AJ, Rohrer DK, Schauble E, Desai KH, Bernstein D, Kobilka BK. Targeted disruption of the beta2 adrenergic receptor gene. *J Biol Chem.* 1999;274:16694-16700.

9. Hardouin SN, Richmond KN, Zimmerman A, Hamilton SE, Feigl EO, Nathanson NM. Altered cardiovascular responses in mice lacking the M(1) muscarinic acetylcholine receptor. *J Pharmacol Exp Ther.* 2002;301:129-137.

10. Henrion D, Terzi F, Matrougui K, Duriez M, Boulanger CM, Colucci-Guyon E, Babinet C, Briand P, Friedlander G, Poitevin P, Levy BI. Impaired flow-induced dilation in mesenteric resistance arteries from mice lacking vimentin. *J Clin Invest.* 1997;100:2909-2914.

11. Domenga V, Fardoux P, Lacombe P, Monet M, Maciazek J, Krebs LT, Klonjkowski B, Berrou E, Mericskay M, Li Z, Tournier-Lasserve E, Gridley T, Joutel A. Notch3 is required for arterial identity and maturation of vascular smooth muscle cells. *Genes Dev.* 2004;18:2730-2735.

12. Besnard S, Bakouche J, Lemaigre-Dubreuil Y, Mariani J, Tedgui A, Henrion D. Smooth muscle dysfunction in resistance arteries of the staggerer mouse, a mutant of the nuclear receptor RORalpha. *Circ Res.* 2002;90:820-825.

13. Rensen SS, Niessen PM, van Deursen JM, Janssen BJ, Heijman E, Hermeling E, Meens M, Lie N, Gijbels MJ, Strijkers GJ, Doevendans PA, Hofker MH, De Mey JG, van Eys GJ. Smoothelin-B deficiency results in reduced arterial contractility, hypertension, and cardiac hypertrophy in mice. *Circulation.* 2008;118:828-836.

22